Current tectonics of northern Cascadia from a decade of GPS measurements

Stéphane Mazzotti,[1] Herb Dragert,[1,2] Joseph Henton,[3] Michael Schmidt,[1] Roy Hyndman,[1,2] Thomas James,[1,2] Yuan Lu,[1] and Michael Craymer[3]

Received 24 June 2003; revised 4 September 2003; accepted 19 September 2003; published 5 December 2003.

[1] Global Positioning System (GPS) measurements to study regional deformation were initiated in northern Cascadia in the late 1980s and early 1990s. On the basis of a decade of GPS data, we derive a crustal velocity field for NW Washington-SW British Columbia. The permanent and campaign GPS velocities are defined with respect to North America in the ITRF2000 reference frame. Velocity uncertainties are estimated using a model of time series noise spectra. This new velocity field is the basis for interpretation of the tectonics of the northern Cascadia subduction system. GPS velocities are interpreted in terms of interseismic loading of the megathrust using different coupling models. Our data confirm that the upper part of the megathrust is nearly fully locked. An exponential model for the downdip transition zone gives slightly better agreement with the data compared to the common linear transition. The landward decrease of forearc strain loading is smaller than predicted by any of the current subduction interseismic models. This could be a consequence of a small (0–3 mm/yr) long-term motion of the southern Vancouver Island forearc, with respect to North America, or of a concentration of interseismic strain across the elastically weaker Cascadia volcanic arc. In northern Vancouver Island, our velocity field supports the existence of an independent Explorer microplate currently underthrusting underneath North America, at least up to Brooks Peninsula. Further north, GPS velocities indicate transient and/or permanent deformation of northernmost Vancouver Island related to the interaction with the Explorer microplate and possibly with the Queen Charlotte transform margin. *INDEX TERMS:* 1206 Geodesy and Gravity: Crustal movements—interplate (8155); 1242 Geodesy and Gravity: Seismic deformations (7205); 1243 Geodesy and Gravity: Space geodetic surveys; 8123 Tectonophysics: Dynamics, seismotectonics; 8150 Tectonophysics: Plate boundary—general (3040); *KEYWORDS:* Cascadia, GPS, tectonics

Citation: Mazzotti, S., H. Dragert, J. Henton, M. Schmidt, R. Hyndman, T. James, Y. Lu, and M. Craymer, Current tectonics of northern Cascadia from a decade of GPS measurements, *J. Geophys. Res.*, *108*(B12), 2554, doi:10.1029/2003JB002653, 2003.

1. Introduction

[2] Global Positioning System (GPS) measurements to determine crustal strain rates were initiated in the northern Cascadia region (US Pacific Northwest and southwestern British Columbia, Canada) more than a decade ago, with the first campaign measurements in 1986 [*Kleusberg et al.*, 1988] and the establishment of permanent stations in 1991 [*Dragert et al.*, 1995; *Dragert and Hyndman*, 1995]. The permanent networks have since expanded to the current 16 stations of the SW British Columbia Western Canada Deformation Array (WCDA) [*Dragert et al.*, 2001] and 29 stations of the Pacific Northwest Geodetic Array (PANGA) [*Khazaradze et al.*, 1999; *McCaffrey et al.*, 2000; *Miller et al.*, 2001; *Svarc et al.*, 2002] (Figure 1). In this article, we provide an analysis of a decade of permanent and campaign GPS data obtained for the Canadian portion of northern Cascadia. We processed and analyzed data for all of the continuous stations of the combined WCDA and PANGA networks to obtain an accurate and consistent regional deformation picture of the subduction margin. The velocities have been defined with respect to stable North America within the ITRF2000 realization of the International Terrestrial Reference Frame (ITRF) [*Altamimi et al.*, 2002]. The estimation of meaningful GPS velocity uncertainties is not straight forward, and we discuss several methods for using models of the time series noise spectrum.

[3] Our new velocity field provides the basis for interpretation of the tectonics and kinematics of the northern end of the Cascadia subduction system and its transition to the Queen Charlotte transform margin. The primary signal in the GPS velocities comes from the interseismic loading of the Cascadia megathrust [e.g., *Savage and Lisowski*, 1991]. We compare the northern Cascadia GPS observations to the predictions of several different models of subduction fault

[1]Pacific Geoscience Centre, Geological Survey of Canada, Sidney, British Columbia, Canada.
[2]Also at School of Earth and Ocean Sciences, University of Victoria, Victoria, British Columbia, Canada.
[3]Gravity and Geodetic Networks Section, Geodetic Survey Division, Ottawa, Ontario, Canada.

0148-0227/03/2003JB002653$09.00

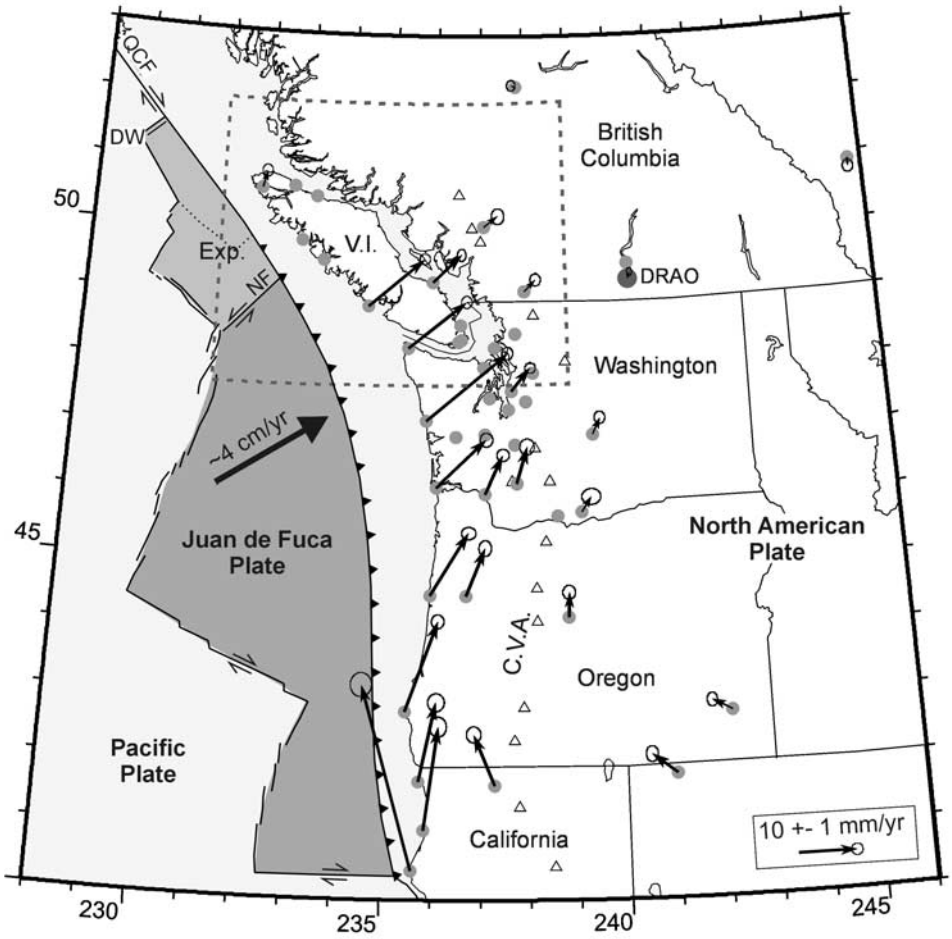

Figure 1. Cascadia permanent GPS network. Gray circles show permanent GPS stations. Reference station DRAO shown as large dark gray circle. Solid arrows show a subset of GPS velocity vectors with respect to stable North America in ITRF2000 (see text). Error ellipses are at 95% confidence level. Juan de Fuca/North America convergence is shown by large black arrow. Open triangles show Cascade Volcanic Arc (CVA) volcanoes. V.I., Vancouver Island; Exp., Explorer microplate; NF, Nootka Fault; DW, Dellwood-Tuzo Wilson Knolls; QCF, Queen Charlotte Fault. Dashed box outlines location of Figure 2.

locking [e.g., *Hyndman and Wang*, 1995; *Wang et al.*, 2003]. The second significant deformation source is the northerly migration and rotation of the Oregon block with respect to North America [*Wells et al.*, 1998; *McCaffrey et al.*, 2000, 2002; *Svarc et al.*, 2002], with a possible extension to NW Washington and Vancouver Island. Off northern Vancouver Island there is a transition from subduction to the Queen Charlotte transform fault, including two microplates or deformations zones, the Explorer Plate and the Winona Block [e.g., *Riddihough*, 1977; *Carbotte et al.*, 1989]. We examine the GPS velocity field to test the existence of an independent Explorer microplate currently underthrusting underneath North America up to Brooks Peninsula, and further to the north, the role of the Winona microplate [*Rohr and Furlong*, 1995; *Kreemer et al.*, 1998].

2. GPS Data and Analysis

2.1. Network Description

2.1.1. WCDA and PANGA Permanent Networks

[4] Continuous GPS data in southwestern British Columbia and the US Pacific Northwest analyzed at the Pacific Geoscience Centre (Geological Survey of Canada, PGC-GSC) are part of two networks: the Western Canada Deformation Array (WCDA [*Dragert et al.*, 1995]) and the Pacific Northwest Geodetic Array (PANGA [*Miller et al.*, 2001]). The WCDA encompasses 16 stations in SW British Columbia and PANGA 29 stations between northern California and northern Washington (Figure 1). In this study, we processed the two networks jointly to provide consistent results for tectonic interpretation of the Cascadia margin. Most of the GPS sites correspond to geodetic monuments, with a forced-centered antenna mounted on a concrete or steel pillar (see http://www.pgc.nrcan.gc.ca/geodyn/wcda/monument.html), or on a steel tripod anchored into bedrock (see http://www.geodesy.cwu.edu/). Exceptions to this rule are the sites from the US Coast Guard GPS network, which have antennas mounted on transmission towers or roofs and may be less stable. Stations are instrumented with dual frequency L1/L2 GPS receivers and antennas from various companies (Ashtech, Trimble, AOA). Most antennas have a "choke ring" design to reduce multipath noise and are equipped with a weather dome.

Table 1a. WCDA-PANGA Permanent Station Velocities

Station	Latitude °N	Longitude °E	V_n,[a] mm/yr	σ_n,[b] mm/yr	RMS,[c] mm	V_e,[a] mm/yr	σ_e,[b] mm/yr	RMS,[c] mm	V_u,[a] mm/yr	σ_u,[b] mm/yr	RMS,[c] mm	T,[d] years
ALBH	48.39	236.51	4.5	0.5	1.4	5.0	0.5	2.0	−0.1	1.0	4.4	6.6
BCOV	50.54	233.16	5.0	0.9	1.4	1.1	0.9	1.6	5.2	2.7	4.9	1.8
BLYN	48.02	237.07	3.8	2.8	3.5	5.5	4.8	6.0	−112.4	18.4	23.0	1.1
BURN	42.78	242.16	1.9	0.6	1.5	−3.4	0.5	1.2	−2.0	1.9	5.5	3.4
CABL	42.84	235.44	15.5	0.6	1.5	5.5	0.5	1.5	0.8	2.0	5.8	3.4
CHWK	49.16	237.99	2.0	0.5	1.2	2.0	0.5	1.2	1.7	1.4	4.4	3.7
CME1	40.44	235.60	31.8	1.1	2.9	−8.8	0.9	2.6	0.0	2.8	8.1	3.4
CORV	44.59	236.70	8.2	0.7	1.7	3.2	0.5	1.6	0.7	1.9	5.6	3.4
CPXF	46.84	237.74	4.9	0.9	1.2	4.9	0.8	1.2	1.0	3.0	4.4	1.4
DRAO	49.32	240.38	1.1	0.4	1.3	0.3	0.2	1.7	0.8	0.3	5.3	6.6
ELIZ	49.87	232.88	5.6	0.8	1.3	3.9	0.9	1.6	6.2	2.7	4.1	2.0
ESQM	48.43	236.57	3.7	0.7	2.0	2.3	0.7	2.0	1.4	1.8	6.8	2.4
FTS1	46.21	236.04	8.2	0.6	1.7	8.5	0.5	2.4	−0.9	1.6	4.9	6.3
GOBS	45.84	239.19	2.6	0.7	2.4	1.7	0.8	3.0	−1.6	1.7	5.8	3.4
GWEN	45.78	238.67	2.6	0.7	1.7	1.9	0.8	2.0	0.5	1.5	6.1	5.0
HOLB	50.64	231.87	2.8	0.5	2.3	0.7	0.5	2.3	2.2	1.4	5.7	6.6
JRO1	46.28	237.78	6.2	0.7	1.5	1.9	0.6	1.9	−0.6	1.5	5.6	5.0
KELS	46.12	237.10	6.6	0.5	1.4	3.0	0.5	1.2	1.2	1.6	4.4	4.6
LIND	47.00	239.46	2.8	0.5	1.4	1.3	0.5	1.3	1.3	1.6	5.1	3.7
LKCP	47.94	238.17	3.1	1.1	1.3	3.5	1.1	1.4	−1.1	5.9	7.4	1.1
NANO	49.30	235.91	4.7	0.5	1.6	4.8	0.4	1.5	1.7	1.1	4.8	6.6
NEAH	48.30	235.38	8.0	0.5	1.7	9.8	0.5	1.9	2.8	1.2	5.3	6.6
NEWP	44.59	235.94	10.7	0.5	1.3	6.5	0.6	1.8	1.4	1.8	5.2	3.4
NTKA	49.59	233.38	7.8	0.8	1.3	7.8	0.8	1.6	5.4	2.5	4.9	2.0
PABH	47.21	235.80	11.6	0.5	1.4	13.7	0.5	1.4	0.0	1.3	4.8	4.9
PGC4	48.65	236.55	4.8	0.7	1.5	4.3	0.8	2.0	2.8	1.7	4.4	2.9
PRDS	50.87	245.71	−1.4	0.5	1.5	0.0	0.5	1.5	0.8	1.4	5.1	4.9
PTHY	50.69	232.63	4.2	1.2	1.5	−0.4	1.3	1.8	2.8	4.8	6.8	1.3
PTSG	41.78	235.75	13.6	0.8	1.6	2.9	0.7	1.6	5.3	2.5	6.1	2.6
PUPU	47.50	237.99	4.9	1.3	1.5	2.2	1.0	1.2	5.4	5.1	6.4	1.1
REDM	44.26	238.85	4.2	0.6	1.4	0.2	0.5	1.4	0.1	1.6	4.6	3.4
RPT1	47.39	237.63	4.0	0.5	1.8	2.8	0.5	2.1	−1.4	1.2	5.3	6.4
SATS	46.97	236.46	8.1	0.6	1.8	5.9	0.6	2.1	1.6	1.5	5.8	5.1
SC00	46.95	239.28	2.6	1.0	1.3	0.6	1.0	1.5	−0.8	3.3	4.9	1.3
SEAT	47.65	237.69	4.0	0.5	1.4	3.2	0.5	1.9	−0.6	1.0	4.7	6.6
SEDR	48.52	237.78	2.8	0.5	1.2	2.5	0.5	1.5	−0.6	1.3	4.7	4.8
SHLD	41.87	240.98	3.4	0.7	1.4	−4.3	0.5	1.3	1.5	2.4	5.8	2.6
SMLD	49.57	240.36	1.4	0.6	1.1	0.3	0.5	1.0	0.4	1.6	3.5	2.2
TRND	41.05	235.85	17.7	0.9	1.9	2.4	0.7	1.7	1.0	2.7	6.4	2.5
TWHL	47.02	237.08	8.6	2.4	3.6	8.7	3.3	4.9	−0.6	6.6	9.8	1.4
UCLU	48.93	234.46	8.2	0.5	1.5	9.3	0.5	1.7	2.0	1.1	5.0	6.6
WHD1	48.31	237.30	5.0	0.8	3.1	4.0	0.7	3.3	−5.1	1.6	7.1	6.4
WILL	52.24	237.83	0.3	0.5	1.4	−0.6	0.4	1.2	2.0	0.9	3.9	6.6
WSLR	50.13	237.08	1.9	0.7	2.6	2.3	0.5	2.0	1.7	1.7	7.1	5.9
YBHB	41.73	237.29	8.8	0.7	1.9	−3.6	0.6	1.9	2.4	2.3	6.8	3.4

[a]Velocity in north, east, and up components.
[b]Modeled uncertainty on north, east, and up velocity components.
[c]Root-mean-square of daily scatter of position in north, east, and up components.
[d]Duration of position time series analyzed.

[5] We have processed the data from the permanent stations from January 1996 to August 2002, ensuring an almost 7-year time series for the few stations that were set up before 1996 (Table 1). The average time span of GPS time series in the continuous networks is 3.9 years with a minimum of 1.1 year and a maximum of 6.6 years.

2.1.2. Vancouver Island Campaign Networks

[6] Four geodetic networks on Vancouver Island comprise 67 sites that were surveyed twice by the Geodetic Survey Division (Natural Resources Canada) with campaign-style GPS occupations during the 1991–1994 and 1996–1999 periods (Figure 2). They usually provide lower accuracy velocities, compared to permanent stations, but allow a greater spatial resolution. Data acquisition method, equipment type, and other parameters (e.g., orbits, frame) vary significantly from one survey to another and from one period to another. However, owing to the large time span (5–6 years) between occupations, the estimated velocities are both spatially coherent and consistent with the nearby permanent stations within the uncertainties.

[7] The Juan de Fuca, Port Alberni, and Central Vancouver Island networks were processed as part of the Ph.D. thesis of Joseph Henton at the University of Victoria and PGC-GSC (see *Henton* [2000] and *Henton et al.* [1999, 2000] for details). The Queen Charlotte Strait network was recently processed at PGC-GSC as part of this study. The Juan de Fuca network is composed of 15 sites in southern Vancouver Island, in the Gulf Islands, and Lower Mainland, BC. The sites were first surveyed in October 1991 and resurveyed in August 1996, with 2–6 occupations of 5–7 hours. The Port Alberni network consists of 21 sites located along a ~50 km wide SW-NE profile running from

Table 1b. Campaign GPS Site Velocities

Site	Latitude	Longitude	V_n,[a]	σ_n,[b]	V_e,[a]	σ_e,[b]	Net,[c]	T,[d] years
ATKI	49.34	236.75	4.0	1.3	4.6	1.5	JdF	4.8
BEEC	48.32	236.35	4.8	0.9	4.9	1.0	JdF	4.8
BONI	48.60	235.28	8.6	1.4	6.2	1.9	JdF	4.8
BOUN	49.08	237.00	4.0	1.2	2.5	1.5	JdF	4.8
CHEM	48.92	236.30	4.9	1.1	4.0	1.2	JdF	4.8
CONS	48.47	236.33	5.1	1.0	4.9	1.1	JdF	4.8
DISC	48.43	236.77	5.2	0.9	2.9	1.3	JdF	4.8
DOUG	48.49	236.65	4.5	0.8	4.6	1.0	JdF	4.8
GABR	49.20	236.18	4.1	3.1	3.2	1.1	JdF	4.8
JORD	48.47	235.90	5.2	1.0	5.2	1.1	JdF	4.8
LAZA	48.61	236.18	5.1	0.9	4.7	1.0	JdF	4.8
RENF	48.56	235.60	6.5	1.3	6.0	1.5	JdF	4.8
SATU	48.78	236.83	3.4	1.2	2.7	1.4	JdF	4.8
SHER	48.38	236.08	5.1	0.9	6.4	1.1	JdF	4.8
YOUB	48.90	235.74	5.9	1.1	4.7	1.3	JdF	4.8
ANDE	49.20	234.97	7.9	1.2	6.8	1.6	PAL	5.1
ARRO	49.22	235.41	6.2	1.2	5.9	1.6	PAL	5.1
FOUR	49.19	234.72	6.5	1.2	5.8	0.9	PAL	5.1
GREY	49.00	235.30	7.0	1.2	6.3	0.9	PAL	5.1
HAND	49.07	235.04	6.4	1.2	5.8	0.9	PAL	5.1
PATL	49.14	235.29	7.8	1.2	6.7	1.6	PAL	5.1
JOAN	49.42	235.08	5.8	1.2	4.7	1.6	PAL	5.1
MARK	49.36	235.27	5.9	1.2	4.0	1.6	PAL	5.1
OKAY	49.23	235.74	5.3	0.7	4.2	0.9	PAL	5.1
BALL	49.35	235.84	5.8	1.2	3.5	1.6	PAL	5.1
TOBY	49.49	235.34	6.1	1.2	4.4	0.9	PAL	5.1
FRED	48.99	234.49	9.2	1.2	8.6	0.9	PAL	5.1
PACH	48.87	234.96	7.5	1.2	7.4	0.9	PAL	5.1
RADA	49.08	234.16	7.2	1.2	8.0	1.6	PAL	5.1
BAMF	48.83	234.87	7.3	1.8	8.0	1.6	PAL	5.1
DAVI	49.60	235.68	5.7	1.2	3.7	0.9	PAL	5.1
SECH	49.60	236.12	4.7	1.2	2.5	0.9	PAL	5.1
SHEP	49.54	235.81	5.0	1.2	3.7	0.9	PAL	5.1
EARL	49.75	236.02	5.0	1.2	2.9	1.6	PAL	5.1
POCA	49.71	235.55	5.1	1.2	2.8	1.6	PAL	5.1
POWE	49.81	235.54	4.6	1.2	3.2	1.6	PAL	5.1
ALEX	49.74	234.51	5.2	1.2	5.2	1.2	CVI	5.1
BCHR	49.65	234.78	3.0	1.6	5.9	1.2	CVI	5.1
GLAC	49.55	234.64	4.0	1.6	6.3	1.2	CVI	5.1
OYST	49.82	234.60	3.7	0.8	3.9	0.8	CVI	5.1
ANAW	49.79	233.45	4.8	1.2	3.7	1.5	CVI	5.1
FILB	49.88	234.30	2.9	0.8	2.7	1.2	CVI	5.1
PIER	49.62	233.88	4.1	1.2	5.1	1.5	CVI	5.1
SENT	49.96	234.04	2.6	1.2	1.9	1.5	CVI	5.1
STRA	50.00	234.42	3.1	0.8	2.4	0.8	CVI	5.1
MOAK	50.10	233.94	2.9	1.2	4.2	1.2	CVI	5.1
ANNA	50.49	234.69	2.1	1.2	2.3	1.2	CVI	5.1
BREW	50.13	234.36	4.3	1.6	5.7	2.6	CVI	5.1
HART	50.03	234.60	2.8	0.8	3.9	0.8	CVI	5.1
HKUS	50.34	234.16	3.6	1.6	2.5	1.2	CVI	5.1
MENZ	50.23	234.50	3.7	1.6	2.1	1.5	CVI	5.1
NACH	49.95	235.00	4.3	1.2	2.4	1.2	CVI	5.1
WASH	49.75	234.70	3.6	1.2	3.0	1.2	CVI	5.1
ALIC	50.46	232.48	2.3	1.1	0.4	0.9	QCS	6.0
BULL	50.96	232.89	3.5	1.3	−0.3	1.2	QCS	6.0
CALV	51.54	232.05	−0.4	1.3	−1.7	1.2	QCS	6.0
COXI	50.81	231.40	2.2	1.3	0.5	1.2	QCS	6.0
HARD	50.70	232.62	0.8	1.4	0.5	1.1	QCS	6.0
JENS	50.65	231.74	1.7	1.3	−1.1	1.2	QCS	6.0
KING	51.85	232.23	1.0	1.3	−2.9	1.2	QCS	6.0
KLUC	50.57	232.84	3.3	1.3	2.1	1.7	QCS	6.0
KOPR	50.49	232.10	1.4	2.2	3.0	1.3	QCS	6.0
ROBI	51.19	232.40	1.4	0.5	−1.1	1.4	QCS	6.0
SCAR	50.65	231.99	0.8	1.2	1.2	0.9	QCS	6.0
SEYM	51.47	232.72	1.9	1.3	0.4	1.2	QCS	6.0
SHUS	50.78	232.19	2.7	1.3	−0.2	1.2	QCS	6.0
SPAT	50.68	231.67	3.9	1.3	0.3	1.2	QCS	6.0

[a]Velocity in north and east components.
[b]Uncertainty on north and east velocity components.
[c]Campaign network: JdF, Juan de Fuca; PAL, Port Alberni; CVI, Central Vancouver Island; QCS, Queen Charlotte Strait (see text).
[d]Time span between the first and second surveys.

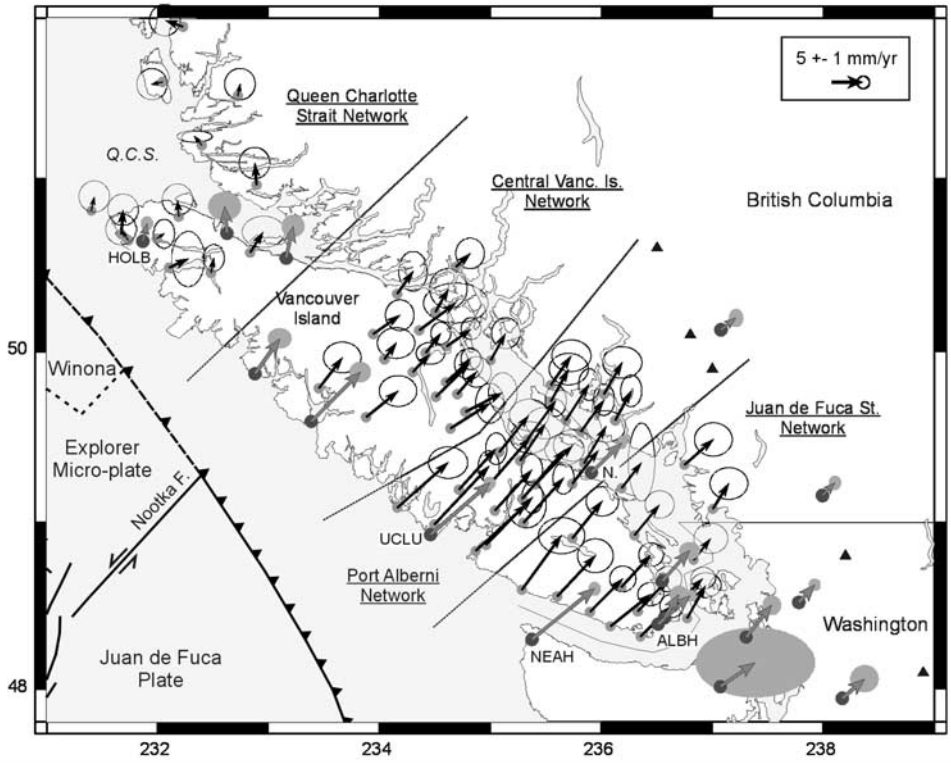

Figure 2. Northern Cascadia continuous and campaign GPS velocities. Thin solid and large gray arrows show horizontal velocities at campaign and continuous GPS sites with respect to stable North America in ITRF2000. Error ellipses are at 95% confidence level. Campaign GPS networks (underlined labels) are separated by thin dashed lines. Q.C.S., Queen Charlotte Strait; Nootka F., Nootka Transform Fault.

the west coast of Vancouver Island to the mainland. It was surveyed in June 1994 with 2–5 occupations of ~6.5 hours and in July 1999 with 2–4 occupations of 4–24 hours. The Central Vancouver Island network consists of 17 sites located between UCLU, NTKA, and the B.C. mainland. The sites were surveyed in July/August 1992 and September 1997 with 2–5 occupations of ~5.5 hours and 4–24 hours, respectively. During the first occupation, the GPS data were affected by testing of antispoofing, leading to increased noise and possible biases in the 1992 network solution. The Queen Charlotte Strait network comprises 14 sites in northernmost Vancouver Island, across the strait on the mainland, and along the Inside Passage. The sites were occupied in July 1993 and in July/August 1999. The first survey was characterized by 2–10 occupations of only 1–4 hours each. For the second survey, sites were occupied 2–6 times for 22–24 hours.

2.2. Processing and Time Series Analysis

[8] The main GPS data processing features are described for the continuous station network. Minor differences in the processing of the campaign data are also described. We carried out the processing at PGC-GSC using the BERNESE 4.2 software [*Hugentobler et al.*, 2001] and the following techniques:

[9] 1. Daily positions are computed using an ionospheric-free, double-difference, phase solution, with station DRAO (Penticton, BC, Figure 1) held as a fixed reference station.

[10] 2. Precise satellite orbits and Earth rotation parameters from the International GPS Service (IGS) are used and held fixed. SIO/SOPAC satellite orbits are used for the campaign data acquired prior to 1994.

[11] 3. Data are sampled at 30 s.

[12] 4. Ocean tide loading corrections are applied using the LOADSTP software [*Pagiatakis*, 1992], which incorporates the FES95.2 global ocean tide model [*Le Provost et al.*, 1998].

[13] 5. Ambiguities are resolved by constraining a regional ionospheric model (''quasi-ionosphere-free'' strategy).

[14] 6. Tropospheric delay corrections are applied using Dry Niell mapping function [*Niell*, 1996] with 24 zenith delay estimates and 4 gradient parameter estimates per 24-hour session.

[15] 7. A priori coordinates of the stations are either defined as their ITRF97 epoch 1998.0 value, or as the value derived by a preliminary processing for stations that are not in the ITRF97 solution.

[16] 8. Changes in antenna models, antenna heights, and phase center corrections are accounted for using IGS phase center calibrations.

[17] We introduced minor differences during the processing of the campaign data, essentially to stabilize the results on some of the short occupation surveys and to ensure a strong tie to the continuous network solution. Depending on the time period, available nearby permanent stations were included in the campaign data analysis and constrained tightly to positions derived from the continuous network analysis (see *Henton* [2000] for details). For the Queen Charlotte Strait network, we used nearby station HOLB

(Holberg, northern Vancouver Island, see Figure 2) as the fixed reference, instead of the more distant DRAO. Tropospheric gradient estimation was turned off because the very short occupations during the first survey did not allow their separation from other parameters.

[18] For the continuous network, we inverted independently the north, east, and up components of the station time series (position u change with time t), using least mean squares regression to constrain the parametric relation:

$$u(t) = a + b\mathrm{t} + c\cos(365.25t + \phi) + [k_1\mathrm{t}_1 + .. + k_i t_i]$$

where a is the intercept, b is the rate of change (velocity) assumed to be constant through time, c and ϕ are the amplitude and phase of a 365.25 day seasonal variation, and k_j is the amplitude of an instantaneous offset at time t_j associated with a change of antenna or dome, or with a large earthquake (e.g., the 2001 Nisqually earthquake).

[19] We obtained the best fit model for the regression parameters through an iterative technique. First, obvious large outliers were eliminated and offsets at all identified times of "disruptions" were estimated. Outlier rejection was then further refined by the removal of data points for which the residual difference from the initial parametric model exceeded three times the standard error of the model fit. Next, each offset estimate that had a magnitude smaller than three times its formal regression error was deemed to be not statistically significant and removed. This removal was done for one offset parameter at a time, with new regressions providing revised estimates for all remaining parameters. This process was repeated until only statistically significant offset estimates remain in the regression.

[20] The discovery of ~2 weeks transient signal in the GPS time series associated with slow slip events [*Dragert et al.*, 2001, 2002] adds an extra level of complication in the modeling of the GPS data to extract long-term rates (significant over several years). The slow slip deformation can be treated in one of two ways: (1) Offsets are introduced at the time of each slow slip event (assuming an instantaneous step) in order to estimate the average velocity of the GPS station between slip events; and (2) no offset is allowed for at the time of the slow slips. Under this scenario, slow-slip events are regarded as short-term perturbations with their own strain loading/release process and make no net contribution to the long-term deformation velocities over a few cycles. We used this second option to estimate the GPS long-term velocities. The assumption of a null deformation budget associated with slow slip events implies that long-term velocities estimated at GPS sites located in the region of the slow slip events and with short (less than 3–4 years) time series are susceptible to a significant bias (up to 1–2 mm/yr).

[21] For the campaign measurements, we estimated the long-term velocity at each site assuming a constant rate between the network surveys. The site velocity corresponds to the weighted best fit linear rate between the daily positions of the two occupations. Because the campaign networks rely on two surveys with a few days of data, seasonal signals and potential offsets could not be estimated. These limitations are considered in the uncertainty budget of the campaign data.

2.3. Estimation of Uncertainties

[22] Studies of the spectral component of GPS time series suggest the noise may be described using a frequency-dependent model with a spectral index between 0.5 and 2. [e.g., *Zhang et al.*, 1997; *Mao et al.*, 1999]. On the basis of the analysis of 3-year-long GPS data, *Mao et al.* [1999] derived an empirical model to describe the noise as function of white (σ_W), flicker (σ_F), and random walk (σ_R) components:

$$\sigma_M^2 \cong \left(12\sigma_W^2\right)/\left(gT^3\right) + \left(1.78\sigma_F^2\right)/\left(g^{0.22}T^2\right) + \left(\sigma_R^2\right)/(T)$$

where g and T are the number of observations per year and the time series length. They estimated the amplitude of the white and flicker noise at 23 global stations and concluded that uncertainties in GPS velocities might be underestimated by factors of 5–11 if pure white noise is assumed.

[23] These results have been adopted by many researchers to describe the uncertainties on GPS velocities (e.g., *Dixon et al.* [2000] for California, *Miyazaki and Heki* [2001] for Japan, *Miller et al.* [2001] for Cascadia, and *Sella et al.* [2002] for global). Variations, however, exist in the implementation of this error model. In particular, the random walk component is frequently neglected, on the basis that it should only become significant for long (4–5 years and more) time series. The amplitude of each noise component can be derived from geographical averages provided by *Mao et al.* [1999]. An alternative, and fairly common, approach consists in exploiting the correlation between these noise parameters and the weighted root-mean square (WRMS) of daily scatter of individual time series. Empirical scaling laws are then derived that provide the amplitude of the white and flicker noise component as a function of the WRMS [*Dixon et al.*, 2000; *Miller et al.*, 2001].

[24] With no colored noise assumption, the formal standard deviation on velocities derived from our continuous station time series are too optimistic (0.0–0.9 mm/yr in the horizontal components and 0.1–3.1 mm/yr in the vertical component) and do not show any significant decrease with the length of the time series. Thus we adopt the empirical error model defined by *Mao et al.* [1999], using the following simple first order scaling factors between the time series WRMS and the different noise components:

White noise $\quad \sigma_W \cong 0.7$ WRMS

Flicker noise $\quad \sigma_F \cong 1.0$ WRMS

Random walk $\quad \sigma_R \cong 0.5$ WRMS

[25] We derived these scaling factors from a comparison of WRMS and noise amplitude for North America GPS studies [*Mao et al.*, 1999; *Dixon et al.*, 2000; *Miller et al.*, 2001]. The first two expressions give a reasonable fit to Mao et al.'s data (within ~0.5 mm/yr). The third expression gives mean σ_R values of 0.9, 1.0, and 3.0 mm/yr$^{1/2}$ in the north, east, and up components, respectively (range of 0.6–1.8, 0.5–3.0, and 1.8–11.0 mm/yr$^{1/2}$). These numbers are in reasonable agreement with the estimates of *Langbein and Johnson* [1997], based on 10 yearlong trilateration time series (σ_R range between 0.5 and 3 mm/yr$^{1/2}$).

Table 2. Uncertainty Scaling Factor[a]

	JdF	PAL	CVI
North	2.7	4.0	1.9
East	4.9	3.1	2.0

[a]JdF, Juan de Fuca network; PAL, Port Alberni network; CVI, central Vancouver Island network.

[26] Given these noise parameters, the estimated uncertainties for the permanent station velocities vary, in the horizontal components, between ~1–1.5 mm/yr for 1 year time series and ~0.5 mm/yr for 5 year and longer time series. The vertical component shows uncertainties that range between ~5 mm/yr and ~1.5 mm/yr for the same respective time spans (see Table 1).

[27] The formal standard error derived from the inversion of the position time series for the campaign data is also too optimistic (~0.4 mm/yr on average) to properly describe the uncertainties on velocities. The actual uncertainties on the campaign velocities should reflect sources of error inherent to campaign GPS and not easily detected because of the few observations. Four potential error sources are considered that lead to an error budget of ~1.2 mm/yr:

[28] 1. Slow slips events can lead to potential biases in the estimated position of as much as 3–5 mm for affected sites [*Dragert et al.*, 2001]. These nearly periodic events are superimposed on the long-term rate. Because of the small permanent GPS coverage prior to 1996, the spatial extent and amplitude of pre-1996 slow slip events is not well constrained [*Dragert et al.*, 2002], thus precluding a correction of pre-1996 campaign surveys. This possible position bias translates into a potential error of 0.5–1.0 mm/yr in the estimated velocity over a 5–6 years time series.

[29] 2. Continuous time series show that changes of antenna type, dome, or skirt, at the reference station can affect the estimation of position of other stations by up to 10 mm in the vertical component. The effect appears to be insignificant (~0.5 ± 0.5 mm) in the horizontal component.

[30] 3. As shown in permanent station analysis, a change of antenna at campaign sites can add a nonmodeled offset of up to 20–30 mm in the vertical component and a few mm in the horizontal. Over a 4–6 years period, this translates into an uncertainty on the horizontal velocity of ~0.5 mm/yr.

[31] 4. The main characteristic of campaign survey is the repeated set up of the GPS antenna over a marker. An overall uncertainty of ~1 mm in the horizontal components is estimated due to the set up variations and tripod deformation during the surveys. For two occupations over 4–6 years, this suggests an uncertainty of 0.3–0.5 mm/yr.

[32] Alternatively, the uncertainties in the campaign velocities can be estimated using the same method as for the permanent network solution: i.e., an error model including white, flicker, and random walk noise [*Mao et al.*, 1999], and WRMS of the daily scatter used to scale the different noise component amplitudes. However, time series with only 1 or 2 occupations during two surveys do not provide a significant estimate of the WRMS. Thus we estimated the uncertainties on the campaign velocities by directly scaling the formal standard errors with empirical constants (Table 2) such that the horizontal uncertainty averaged about 1.2 mm/yr for each network.

2.4. Adjustment to ITRF2000 and North America

[33] The analysis of the derived position time series allows high accuracy estimation of station velocities with respect to the reference station [cf. *Dragert et al.*, 2001]. However, this procedure has some disadvantages over the free-network adjustment strategy, mostly because our fixed reference-station strategy does not allow for a possible motion of the reference station DRAO within the analysis reference frame. Three issues arise when our rates are used for comparison with other studies or with various crustal deformation models:

[34] 1. Our reference station DRAO likely has a small velocity with respect to stable North America (up to 2 mm/yr roughly northeastward [e.g., *Miller et al.*, 2001]).

[35] 2. A slight network distortion is induced during the processing by fixing a reference station that has a large velocity (~17 mm/yr) in the ITRF reference frame (frame used for the definition of the GPS satellite orbits). This distortion increases linearly with the distance to the reference station, from ~0.1 mm/yr at 500 km to ~0.3 mm/yr at 1000 km in the horizontal components, and from ~0.6 mm/yr to ~1.2 mm/yr for similar distances in the vertical component.

[36] 3. The original velocities are not attached to any particular ITRF realization.

[37] To account for these biases, we derived an empirical procedure that allows mapping the original velocities into a given ITRF realization and a given stable North America reference. We map GPS velocities into the ITRF2000 realization [*Altamimi et al.*, 2002], which is the most recent and most robust realization of the ITRF. We use empirical transfer functions that describe the effect on the velocity of every station due to the motion of the reference station (DRAO). The network adjustment to ITRF2000 is estimated by solving for the velocity of DRAO that minimizes the difference in horizontal and vertical velocities for a subset of 14 common stations between our solution and the ITRF2000 solution. The best fit DRAO velocity agrees with the velocity from the ITRF2000 solution within 0.6 mm/yr (Table 3). The velocities for the continuous and campaign networks are then mapped into ITRF2000 by propagating the velocity of DRAO, and the associated uncertainties, to the other stations.

[38] There is a significant difference of ~2 mm/yr between the velocity of DRAO in ITRF2000 and in ITRF97 (Table 3). A similar difference is found for ALBH and WILL (the only well constrained Cascadia stations in ITRF97 solution). Because these three stations have long time series (~7 years) and are among the core ITRF sites, this difference probably reflects an actual variation in the ITRF realization, rather than fluctuation of these partic-

Table 3. DRAO Velocity in ITRF

	$V_n \pm \sigma_n$[c]	$V_e \pm \sigma_e$[c]	$V_u \pm \sigma_u$[c]
ITRF2000 adjustment[a]	−11.7 ± 0.3	−14.0 ± 0.1	0.8 ± 0.3
ITRF2000 solution[b]	−11.7 ± 0.5	−13.4 ± 0.3	1.2 ± 0.5
ITRF97 solution[b]	−13.2 ± 0.5	−12.6 ± 0.4	0.5 ± 0.6

[a]Adjustment of 14 permanent common stations and ITRF2000.
[b]Nominal ITRF2000 and ITRF97 solutions.
[c]Velocity and standard error (1σ) in north, east, and up components in mm/yr.

Table 4. Predicted Velocities for Different NA/ITRF Rotation Vectors

	Penticton		Holberg		Cape Mendocino	
Location	V_n	V_e	V_n	V_e	V_n	V_e
ITRF2000[a]	−12.8	−14.3	−15.2	−13.0	−14.2	−11.9
ITRF97[b]	−14.0	−12.2	−16.3	−10.8	−15.3	−9.5
ITRF96[c]	−13.7	−12.7	−16.0	−11.2	−15.0	−10.1

[a]After *Altamimi et al.* [2002].
[b]After *Svarc et al.* [2002].
[c]After *DeMets and Dixon* [1999]. North and east velocities in mm/yr.

ular stations. Our solution mapped in ITRF97 would thus be significantly different from our preferred ITRF2000 solution.

[39] Because the Queen Charlotte Strait campaign network was processed with respect to station HOLB, the adjustment of the velocities to ITRF2000 is done in a similar way as for the other networks, but using the ITRF2000 velocity of HOLB rather than that of DRAO.

[40] The continuous and campaign solutions, mapped into ITRF2000, are then transformed into solutions with respect to stable North America (NA) by removing the predicted velocity at each station associated with a given NA/ITRF2000 rotation vector. Various NA/ITRF rotation vectors exist that reflect the different realizations of the ITRF and the numerous solutions for North America scale GPS networks. Although they all agree to a first order, small differences arise that feed into the predicted motion of North American sites (Table 4). In order to be consistent with the choice of the ITRF2000 as a reference frame, we use the NA/ITRF2000 rotation vector as defined by *Altamimi et al.* [2002] for transformation to North America reference. This rotation vector is based on velocities of 16 stations in stable North America, directly derived from the ITRF2000 solution, and thus includes a combination of GPS, VLBI, and SLR rates.

[41] The NA/ITRF2000 vector used is -5.04 ± 1.14°N, 276.86 ± 1.95°E, -0.194 ± 0.003°/Myr (latitude, longitude, rotation rate positive counterclockwise). The uncertainties are formally propagated to the final velocities (uncertainties on this rotation vector correspond to uncertainties on velocities at sites in Cascadia of ~0.1–0.3 mm/yr). The final horizontal velocity field for northern Cascadia is shown on Figure 2.

2.5. Consistency Between the Campaign and Permanent Solutions

[42] The consistency between the solutions for the different campaign networks and the permanent networks can be estimated by comparing the velocities of nearby campaign and permanent sites. The combined campaign-continuous velocity field shows good agreement between the elements of this combination, both in magnitude and direction of the velocity vectors (Figure 2). However, there are suggestions of small systematic differences among the survey networks:

[43] Of the four campaign networks, the Juan de Fuca network shows the best agreement with the permanent solution. This is likely due to the fact that it is the only campaign network constrained by surrounding permanent stations during both surveys.

[44] There is an indication for a small (5–10°) counterclockwise rotation of velocities for inland sites of the Port Alberni network, compared to the Juan de Fuca and to the UCLU and NANO velocities.

[45] The internal scatter in the solution for the Central Vancouver Island network is slightly larger than that for the two other campaign networks on southern Vancouver Island. This larger scatter may be related to the testing of antispoofing on GPS signal during the 1992 survey.

[46] For the Queen Charlotte Strait network, where both ALBH and DRAO stations were processed and analyzed in the campaign-style mode, the campaign velocities derived for those two stations agree with the permanent solution at the 95% confidence level, with differences of 1.1 and 0.5 mm/yr, respectively. These comparisons indicate that there is an overall agreement between the campaign solutions and the continuous solution. In most cases, this agreement is better than 1 mm/yr, with some discrepancies up to 2–3 mm/yr.

3. Southern to Central Vancouver Island: Subduction Regime

3.1. Tectonic Setting

[47] The increase in geodetic coverage of the Cascadia margin has led, over the last few years, to an increase in studies of forearc deformation and its relationship to the subduction interseismic loading. Early work was mostly based on locally limited leveling and trilateration-triangulation measurements [e.g., *Reilinger and Adams*, 1982; *Savage et al.*, 1991; *Dragert et al.*, 1994]. In contrast, more recent studies include tens of campaign and permanent GPS sites over the whole Cascadia margin [*McCaffrey et al.*, 2000; *Miller et al.*, 2001; *Svarc et al.*, 2002]. The most recent efforts involve establishing hundreds of campaign sites from Oregon to southern British Columbia [*McCaffrey et al.*, 2002].

[48] Owing to these geodetic studies and to extensive seismicity and tectonic studies [e.g., *Riddihough*, 1984; *Walcott*, 1993; *Wells et al.*, 1998], the main aspects of the present-day Cascadia tectonics and dynamics are well constrained: The subduction thrust is currently fully or close to fully locked, leading to margin-normal shortening and uplift of the forearc [e.g., *Dragert and Hyndman*, 1995; *Miller et al.*, 2001]; The Oregon part of the forearc is migrating northward at 5–10 mm/yr, with little internal permanent deformation [*Wells et al.*, 1998; *McCaffrey et al.*, 2000; *Svarc et al.*, 2002]; Superimposed on the subduction transient signal, the Puget Sound-southern Georgia Strait region of the forearc is affected by permanent north-south shortening [*Khazaradze et al.*, 1999; *Mazzotti et al.*, 2002].

[49] The details of this tectonic picture are still being discussed and improvements in the spatial coverage and the resolution of the GPS data should help address issues such as (1) the distribution of interseismic coupling (extent of locked zone, time variation, coupling ratio), (2) the characteristics and spatial pattern of slow slip events, (3) the distribution of permanent deformation in the northern Cascadia forearc (e.g., rotation vector versus distributed strain), and (4) the relationship of forearc steady N-S deformation to the transient megathrust earthquake cycle.

Table 5. Time Variation of Juan de Fuca/North America Convergence

	Rotation Vector			Predicted Velocity (48°N, 234°E)			
Model [a]	Latitude °N	Longitude °E	ω,[b] deg/Myr	V_n, mm/yr	V_e, mm/yr	V, mm/yr	Azimuth, °N
3 Ma (NUVEL-1A)	22.40	247.19	−0.831	19.5	38.3	42.9	63.0
1.9 Ma (W&D)	29.16	246.25	−0.984	20.3	33.7	39.3	59.0
0.8 Ma (W&D)	32.76	243.68	−1.241	19.5	35.1	40.1	60.9
0.4 Ma (W&D)	35.28	243.63	−1.504	22.8	35.4	42.1	57.2
0.0 Ma (extrapolated)	37.80	243.60	−1.750	25.6	32.9	41.7	52.0

[a]NUVEL-1A [*DeMets et al.*, 1994]; W&D, combination of Juan de Fuca/Pacific [*Wilson*, 1993] and Pacific/North America [*DeMets and Dixon*, 1999].
[b]Rotation rate (positive counterclockwise).

[50] The interpretation for SW British Columbia and NW Washington of our GPS velocity field addresses some of these issues using recent developments on plate convergence and the earthquake cycle. Our starting point is that the deformation observed by GPS in SW British Columbia is mostly controlled by the interseismic loading of the margin. The consequences of small continuous forearc deformation are discussed later in section 3.4. Two models of interseismic coupling are considered; both use the concept of dislocation in an elastic half-space:

[51] Model 1 is a standard 3-D model, where the locked and transition zones are defined on the basis of thermal and geodetic constraints [*Hyndman and Wang*, 1995]. The transition zone has approximately the same width as the locked zone and is defined by a linear downdip decrease of the coupling [*Flück et al.*, 1997].

[52] Model 2 is a more recent 3-D model, where the extent of the transition zone was revisited on the basis of modeled viscoelastic behavior of the subduction system after megathrust earthquakes [*Wang et al.*, 2002]. The transition zone is twice larger than for model 1 and is defined by an exponential downdip decrease of the coupling.

[53] Another source of variations in the modeling and interpretation of the GPS deformation field is the subduction velocity between the Juan de Fuca plate and the Cascadia forearc. There are several models that describe the relative plate motion in the region, involving the Juan de Fuca (JF), Pacific (PA), and North America (NA) plates, and the Oregon forearc sliver. Because we are primarily interested in deformation in northern Cascadia (i.e., north of the Puget Sound deformation zone), the migration of the Oregon forearc is not considered. The global relative plate motion model NUVEL-1A [*DeMets et al.*, 1994] provides a JF/NA rotation vector that is averaged over the last 3 Myr. A recent study combining GPS and geologic evidence concluded that the current PA/NA motion is faster than predicted by NUVEL-1A [*DeMets and Dixon*, 1999]. Additionally, *Wilson* [1993] found a series of significant changes in the JF/PA rotation vector during the last 3 Myr. To test the impact of these variations on the subduction velocity, three JF/NA rotation vectors were derived from *Wilson* [1993] (1.9, 0.8, and 0.4 Ma, Table 5). A hypothetical rotation vector at 0 Ma was extrapolated from the 1.9–0.4 Ma pattern of change.

[54] In spite of the clear northwestward migration of the rotation pole, the associated increase in the rotation rate translates into very small variations of the predicted subduction rate at 48 °N. The subduction direction is affected by a small counterclockwise rotation of ∼10° between 3 and 0 Ma (Table 5). The most recent JF/NA rotation vector (0.4 Ma) was used in the standard interseismic model discussed below.

3.2. Interseismic Loading and Horizontal GPS Velocities

[55] The velocity fields predicted by both interseismic loading models (linear and exponential) explain the first order pattern of the GPS horizontal velocities: northeastward motion and landward decreasing rates from 15–10 mm/yr along the west coast to 3–5 mm/yr inland. The goodness of fit of the models is estimated using a reduced chi square estimator:

$$\chi^2_N = \left\{ \Sigma_N \Sigma_2 (V_G - V_M)^2 / \sigma^2_G \right\} / df$$

where V_G and V_M are the GPS and modeled horizontal velocities at each station, σ_G is the uncertainty on the GPS velocity, and df is the number of degrees of freedom in the system (i.e., number of observations minus number of unknowns, in this case the length of the transition zone is assumed to be the only unknown). The χ^2_N is a measure of how well a given model explains the variance in the data set within the uncertainties on the data. Hence $\chi^2_N \gg 1$ implies a poor fit and/or an underestimation of the data uncertainty.

[56] The χ^2_N for both models estimated for the continuous and campaign stations are shown in Table 6. Model 2 (exponential decrease) shows a small but systematic ∼25% improvement of fit compared to model 1 (linear decrease). The χ^2_N for the permanent stations is significantly larger than 1, indicating either a poor fit of both models and/or an underestimation of the GPS uncertainties by a factor of ∼2.5.

Table 6. The χ^2_N of Model Misfit

	All[a]	Continuous[b]	Campaign[c]
Model 1 (linear)	3.6	8.2	2.5
Model 2 (expo.)	2.6	6.3	1.8
Model 2b (0 Ma)[d]	2.1	4.8	1.4
Model 3 NE[e]	3.0	10.4	1.3
Model 3 NW[e]	4.7	13.3	2.7

[a]Campaign and permanent stations in northern Cascadia.
[b]Subset of permanent stations including ALBH, CHWK, DRAO, ESQM, NANO, NEAH, NTKA, PGC4, SEDR, SMLD, UCLU, WHD1, WSLR.
[c]Stations from the campaign networks.
[d]Similar to model 2 with 0 Ma rotation vector (Table 5).
[e]Similar to model 2 with imposed Vancouver Island forearc motion (see section 3.4).

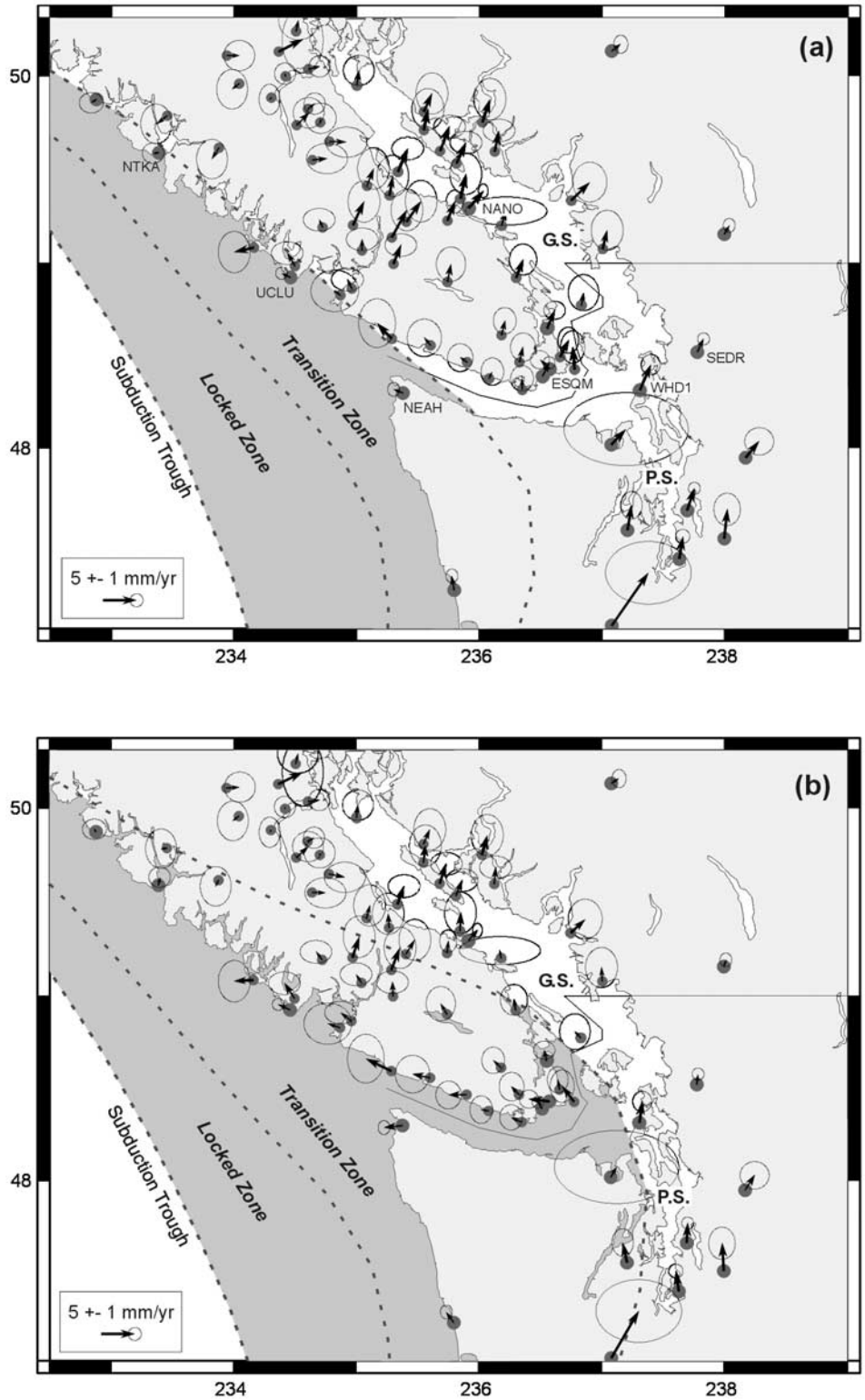

Figure 3. Residual GPS velocities. Solid arrows show residual horizontal velocities (after correction for modeled subduction interseismic deformation) with respect to stable North America in ITRF2000. Error ellipses are at 95% confidence level. Light gray shading indicates locked and transition zones of the subduction thrust. G.S., Georgia Strait; P.S., Puget Sound. (a) Residual velocities for model 1, short linear downdip transition zone; (b) model 2, wide exponential downdip transition zone (see text).

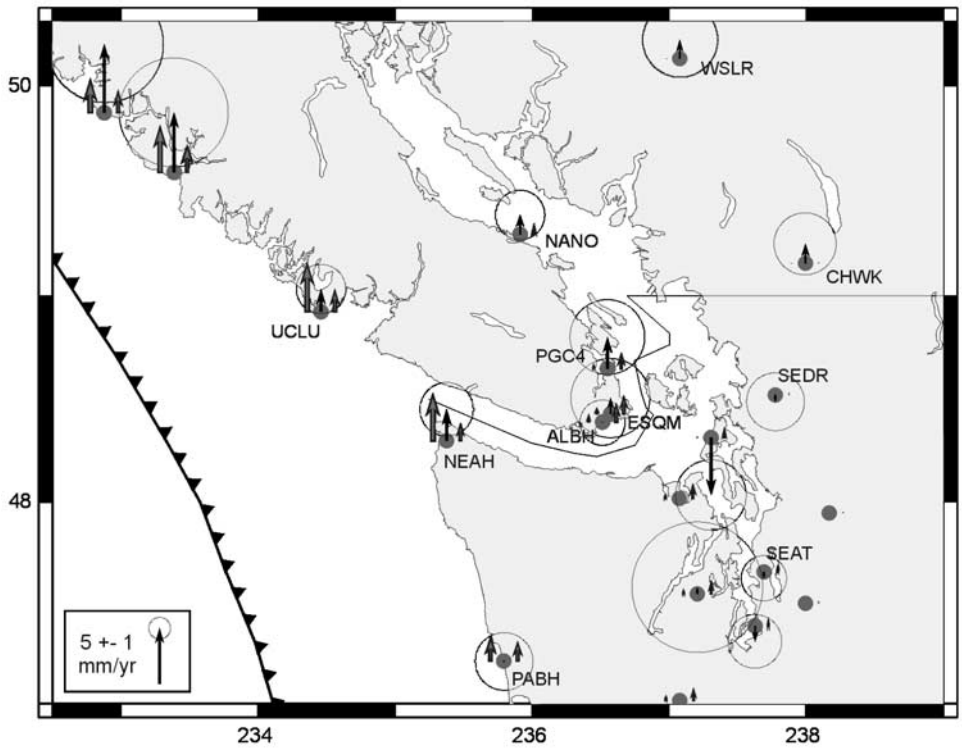

Figure 4. GPS and model vertical velocities. Solid arrows show vertical GPS velocities (north, up; south, down) for permanent stations with respect to stable North America in ITRF2000. Error ellipses are at 95% confidence level. Gray shaded arrows left and right of solid arrows show vertical velocity predicted at GPS site by models 1 and 2, respectively.

[57] The residual velocity vectors (Figure 3) show some locally coherent geographical patterns. For both models, inland sites in southern central Vancouver Island show a consistent northeastward residual velocity of 1–2 mm/yr. This suggests a smaller tapering out of the subduction loading (e.g., wider locked and/or transition zone). For model (2), sites on the west coast of southern Vancouver Island show a northeastward residual velocity of 1–2 mm/yr (Figure 3b), reflecting a $\sim$10° difference in azimuth between the GPS velocities and the predicted displacements. This residual pattern can be reduced by introducing the 0 Ma JF/NA rotation vector to control the subduction direction and rate (see Table 5). The χ^2_N for this alternative model 2b shows an improvement of fit of $\sim$20% compared to model 2 and $\sim$40% compared to model 1. The change in subduction direction does not significantly affect the fit for the central Vancouver Island stations (sites farther away from locked fault).

[58] Although the fit to the permanent GPS stations was improved by the introduction of the 0 Ma rotation vector, the χ^2_N is still significantly larger than 1. One implication is that the GPS uncertainties are too small and should be scaled by $\sim$2.2. Alternatively, a closer look at the residual velocities and the contribution of each station to the total χ^2_N indicates that, out of the 13 sites, 5 have significantly larger residuals: SEDR and WHD1 (likely affected by permanent margin-parallel deformation), NANO, ESQM (only 2.4 yr of data), and NEAH. Removing these stations from the subset leads to a more reasonable $\chi^2_N \approx 2.2$.

[59] This analysis of the GPS misfit suggests that the subduction loading model can be slightly improved by a more northward subduction direction (by 5–10°) and by a slower landward decrease of the interseismic loading, especially along the Port Alberni corridor. The reduced strain gradient along the Port Alberni corridor could be due to systematic variations in the rheology of the inner arc or to long-term forearc motion, as discussed in sections 3.3 and 3.4, respectively.

3.3. Vertical Deformation

[60] Because early campaign surveys consisted in a few 5–7 hour-long occupations, we do not consider the vertical results of the campaign networks. The main conclusion from the analysis of the vertical velocity at permanent stations is that most of the rates are not significant at the 95% confidence level (Figure 4 and Table 1). The vertical velocities are small, between −2 and 2 mm/yr for the long time series (3 years or more) and the associated uncertainties are large, 1–1.5 mm/yr at 1σ. Hence the χ^2_N for the vertical solution is identical ($\chi^2_N \approx 1.4$) for any model considered, even for a no-subduction model.

[61] Nevertheless, there are significant differences between model 1 and model 2 that can be compared to the GPS vertical pattern. In particular, the GPS velocities suggest that the landward tilting of the forearc is not as large as the subduction loading models predict (Figure 4). Vertical velocities across southern Vancouver Island show an even uplift at $\sim$2 mm/yr, with a very small tilt (0.3–1.0 mm/yr) between the west coast and the mainland. This regional small to insignificant landward tilt favors model 2, which shows a much smaller tilt than model 1. Combined with the analysis of the horizontal GPS residuals, this vertical pattern

supports the conclusion that the landward decrease of the subduction-loading signal is slower than predicted by model 2, especially for the central Vancouver Island section.

[62] On average GPS vertical velocities in southern Vancouver Island are 1.3 ± 1.5 mm/yr larger than model 2 predictions (Figure 4). This higher uplift rate and the lack of landward tilt discussed previously might be associated with current postglacial rebound (PGR) signal. PGR corrections vary significantly depending on the model used [e.g., *James et al.*, 2000]. The most recent study [*Clague and James*, 2002] suggests that PGR uplift rates for northern Cascadia could range between 0.5 and 0.8 mm/yr, with a small seaward tilt across Vancouver Island of 0.1–0.2 mm/yr. These PGR corrections could account for part of the discrepancy between our GPS velocities and the interseismic loading model.

[63] It should be noted that these conclusions from the GPS residuals, and their implications on the subduction interseismic loading, are based on second order features of both the GPS data and the subduction model. To a first order the GPS velocities can be well explained by the simple uniform elastic half-space loading models. Although it may be possible to extract important information from the small misfits, rather than trying to force a perfect match between the GPS velocities and the models, the limitations of these simple models and the need for more complex models should be considered. For example, variations in elastic properties of the medium can induce significant perturbations in the predicted deformation field [cf. *Cattin et al.*, 1999]. Recent analysis of releveling data across central Vancouver Island and the adjoining inner coastal margin to the east has identified a broad region of uplift coincident with the Cascade volcanic belt [*Wolynec et al.*, 2003]. It is conceivable that this region of high heat flow [*Lewis et al.*, 1992] has resulted in a weaker crustal zone, which accommodates an anomalous proportion of regional interseismic loading. This can account for the reduced horizontal strain gradient and the more uniform uplift of the coastal margin to the west of the volcanic belt.

3.4. Long-Term Deformation of the Forearc

[64] Our analysis of the northern Cascadia GPS velocities assumed that the forearc is not affected by significant long-term deformation. In this section, we test the hypothesis of a small permanent motion of the forearc and the potential implications for the subduction interseismic coupling. We use two possible models of motion of the Vancouver Island-northernmost Washington (VI) forearc with respect to North America (NA):

[65] 1. The VI/NA motion is 1–5 mm/yr northeastward. This model would correspond to the hypothesis of a separate Washington block rotating clockwise with respect to North America, at a rate slower than the Oregon block [*McCaffrey et al.*, 2002].

[66] 2. The VI/NA motion is 1–5 mm/yr northwestward. This is supported by the small consistent residual velocities in southern Vancouver Island, which show a NW motion of 1–2 mm/yr (Figure 3b), and by evidence for NW-SE horizontal compression in this region [*Mulder*, 1995; *Currie et al.*, 2001].

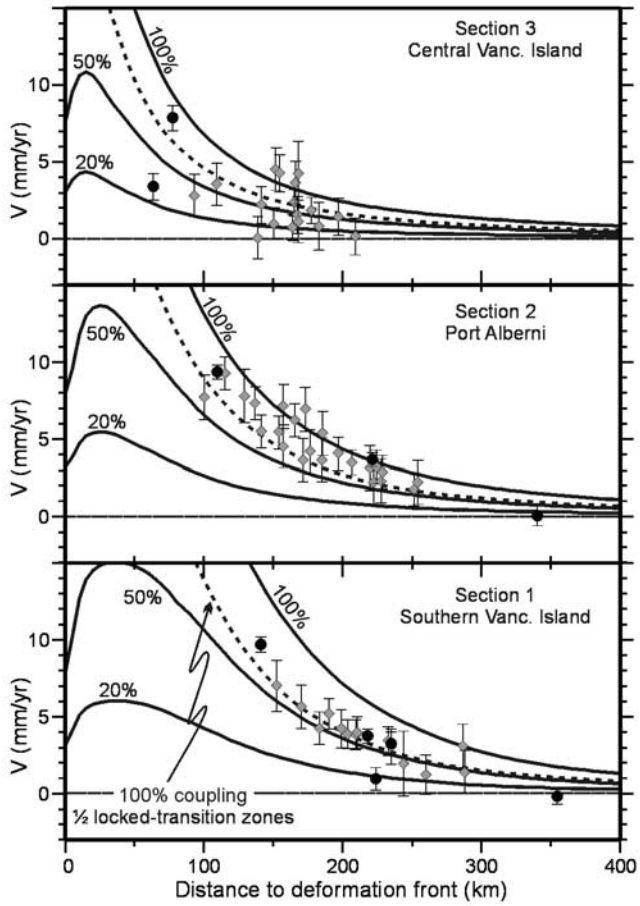

Figure 5. Northeastward moving forearc hypothesis. Margin-normal sections of GPS velocities with respect to southern Vancouver Island-northernmost Washington forearc move 3 mm/yr NE (with respect to North America, see text). Solid circles and shaded squares represent continuous and campaign GPS velocities projected along three N045°E sections. Labeled curves show velocity predicted by subduction-loading model 2 for 100%, 50%, and 20% coupling. Dashed curves show velocity predicted by model 2 for 100% coupling and locked and transition zones reduced to half size.

[67] In both cases, we derive a revised set of GPS velocities (with respect to the VI forearc) that we model using the interseismic loading model 2 (see section 3.2) with a modified subduction velocity accounting for the forearc motion (JF/VI = JF/NA - VI/NA).

[68] Because the plate convergence is almost normal to the subduction trench direction and subparallel to the GPS velocity field, a small northeastward motion of the forearc could easily be mistaken for subduction interseismic loading signal. The impact of a 3 mm/yr NE velocity of the forearc is shown on three margin-normal cross sections (Figure 5). GPS velocities with respect to the forearc decrease from 7–9 mm/yr along the coast to ~0 mm/yr in the Strait of Georgia. Although the convergence rate is reduced by the forearc motion (from 42 mm/yr to 39 mm/yr), these velocities require a low megathrust coupling (~50%, Figure 5). Alternatively, full coupling along significantly smaller

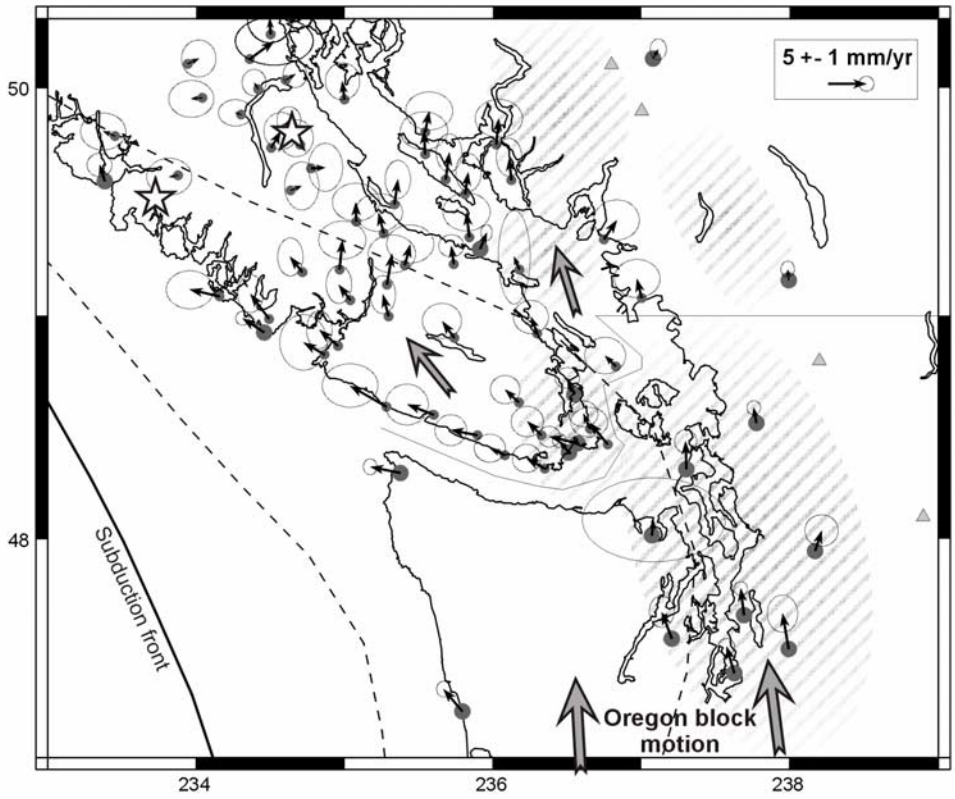

Figure 6. Northwestward moving forearc hypothesis. Residual GPS velocities, with respect to North America, are after correction for interseismic subduction signal but not for imposed 3 mm/yr NW motion of the southern Vancouver Island forearc (see text). Large open stars show $M\sim7$ 1918 (east) and 1946 (west) Vancouver Island earthquakes. Zones of active crustal seismicity are highlighted by light gray shading.

locked and transition zones (width reduction of ~50%, Figure 5) can also be used to match the revised GPS data.

[69] For the whole GPS network, the fit of this partial coupling model is similar to that of the original full coupling (see model 3 NE versus model 2, Table 6). However, the permanent stations show a χ^2_N roughly double compared to the original model. This significant degradation of the model adjustment is mostly associated with the three stations DRAO, NEAH, and UCLU. Without these stations, the adjustment ($\chi^2_N = 4.2$) becomes similar to that of model 2.

[70] A 3 mm/yr northwestward motion of the forearc with respect to North America implies a clockwise rotation of the JF/VI convergence of ~4°, with very little change of the subduction rate. GPS velocities with respect to the forearc also show a more easterly direction that is matched by the interseismic subduction model in southern Vancouver Island-northernmost Washington. In central Vancouver Island the direction of the model-predicted velocities remain more margin normal because of the smaller inland extent of the locked zone (Figure 6). Along the west coast, the residual GPS velocities (corrected for the transient subduction signal but not for the imposed forearc motion) show a northwestward motion of 2–3 mm/yr, with respect to North America, that rotates to a more northerly direction around the Strait of Georgia (Figure 6).

[71] The χ^2_N estimates for this northwestward moving forearc model are ~80% larger than those for the standard model with no forearc motion (see model 3 NW versus model 2, Table 6). As for the NE motion model, the large misfit is essentially due to three permanent stations (DRAO, NANO, and WSLR). Without these three stations, the misfit is only increased by ~20%.

[72] Although these tests of potential forearc motion are crude, they indicate that there may be a small northward (NW to NE) permanent motion of the Vancouver Island-northernmost Washington forearc. The χ^2_N estimates for the moving forearc models suggest that a roughly similar quality of fit can be obtained for a moving forearc model compared to our original stable forearc approach. However, in both models some of the permanent stations are associated with a large deterioration of the model adjustment. The most significant increase of the misfit are found for five of the most robust permanent station velocities derived from ~6 yearlong time series. This suggest that the potential relative motion of the northern Cascadia forearc is not likely to occur as a simple rigid block motion, as we modeled it, and that instead, additional unmodeled processes or local tectonic complications probably occur.

[73] Two main arguments suggest that, if the Vancouver Island-northern Washington forearc is moving with respect to North America, the motion could not be more than a few millimeters per year:

[74] 1. A larger NE motion would require low interseismic coupling and/or narrow locked and transition zones. Although it is not clearly ruled out, we consider that partial

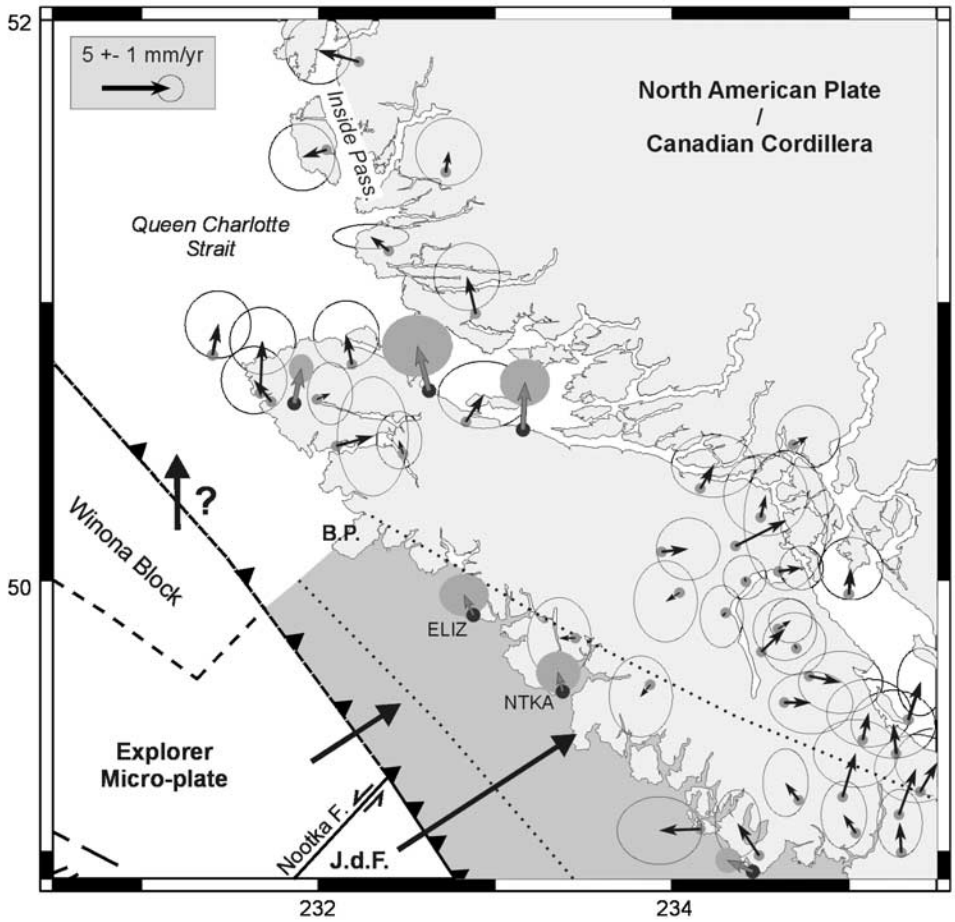

Figure 7. Northern Vancouver Island residual velocities. Thin solid and large gray arrows show horizontal residual velocities (after correction for subduction interseismic transient) at campaign and continuous GPS sites with respect to stable North America. Error ellipses at 95% confidence level. Light gray shading indicates locked and transition zones of the subduction thrust southeast of Brooks Peninsula (B.P.) Dotted lines show the landward limits of the locked and transition zones. Large solid arrows show convergence between North America plate and Juan de Fuca (J.d.F.), Explorer microplate, and hypothetical Winona Block.

coupling is unlikely along the northern Cascadia megathrust. Analysis of geodetic data along many subduction zones generally suggest that strong to nearly full coupling of the seismogenic zone is a fairly common feature [*Mazzotti et al.*, 2000; *Fletcher et al.*, 2001; *Yoshioka et al.*, 2001; *McCaffrey*, 2002]. The downdip extent of the locked and transition zones is well constrained by thermal modeling of the subducting slab [*Hyndman and Wang*, 1995]. The thermal models allow for small variations in the transition isotherm ($\sim$350°C) of a few tens kilometers, but a reduction of 50% would produce a large mismatch between the model and heat flow data [*Hyndman and Wang*, 1993; *Oleskevich et al.*, 1999].

[75] 2. A roughly northward migration of the northern Cascadia forearc has to be accommodated by permanent deformation at the northeastern end of the moving block (central Vancouver Island, Strait of Georgia, and Coast Mountains). The background seismicity level in this region (rate of M $\geq$ 5 earthquake $\sim$1/35 year) and the occurrence of two large $M\sim$7 earthquakes in the last 100 years could be associated with small crustal deformation [cf. *Hyndman and Weichert*, 1983]. By comparison, part of the Oregon block motion is accommodated in the Puget Sound area (3–4 mm/yr [*Mazzotti et al.*, 2002]), producing significant seismicity (rate of $M \geq 7$ $\sim$1/400 year [*Hyndman et al.*, 2003]) and Holocene faulting [e.g., *Atwater and Moore*, 1992; *Johnson et al.*, 1994].

4. Northern Vancouver Island: Subduction-Transform Fault Transition

4.1. Tectonic Setting

[76] The northernmost Cascadia region corresponds to a transition between the subduction of the Juan de Fuca slab to the south and the Pacific-North America transform motion to the north. This transition region is located between two triple junctions that mark the limits of the Explorer (EX) microplate (Figures 1 and 7): The Nootka T-T-F junction between the Cascadia subduction trench, the Explorer underthrusting trough, and the Nootka transform; and the Dellwood T-R-F junction between the Explorer underthrusting trough, the Dellwood-Tuzo Wilson Knolls spreading system, and the Queen Charlotte transform fault.

[77] The current understanding of relative motion between the Explorer microplate and the neighboring plates varies significantly from one boundary to the other. Along the southeastern edge, the JF/EX motion is accommodated along the Nootka Fault [*Hyndman et al.*, 1979]. Seismicity and seafloor reflection profiles indicate a broad zone of shear, rather than a single fault, that accommodates a few cm/yr of left-lateral strike-slip motion [*Hyndman and Weichert*, 1983]. The western edge of the Explorer microplate is bounded by a system of spreading ridges and transform faults that accommodate the EX/PA motion. Earthquake distribution and focal mechanisms correspond to a broad zone of distributed right-lateral shear that cut through the eastern side of the ridge-transform system within the Explorer microplate [*Wahlström and Rogers*, 1992; *Braunmiller and Nábělek*, 2002]. To the northeast, the nature of the present EX/NA relative motion is poorly constrained. There are no clear interplate earthquakes along this boundary. From offshore tectonic data, the Winona block appears to be tectonically and kinematically independent from the Explorer microplate [*Davis and Riddihough*, 1982], whereas earthquake slip vectors suggest the opposite [*Ristau et al.*, 2002; *Braunmiller and Nábělek*, 2002].

[78] Plate reconstruction models suggest that the Explorer microplate separated from the Juan de Fuca plate ~3.5 Ma [*Riddihough*, 1977]. At this time, the Nootka Fault became active (at about its present location) and the T-R-F triple junction jumped northward from Brooks Peninsula to its present position. The location of the northern edge of the subducted slab follows a NE-SW line (Figure 7) constrained by plate reconstruction models [*Riddihough*, 1977], heat flow data, magnetic, and gravity anomalies [*Lewis et al.*, 1997], and seismic velocity receiver functions [*Cassidy et al.*, 1998].

[79] Two end-member models of the current EX/NA plate tectonics have been proposed:

[80] 1. The Explorer region forms an independent microplate underthrusting underneath northern Vancouver Island at a rate slower than the JF/NA motion off southern Vancouver Island. This option is supported by plate motion models based on magnetic anomalies and earthquake slip vectors [*Riddihough*, 1984; *Riddihough and Hyndman*, 1989; *Ristau et al.*, 2002; *Braunmiller and Nábělek*, 2002].

[81] 2. The Explorer region does not correspond to an independent plate anymore. In this model, the full PA/NA motion is accommodated along the Queen Charlotte Fault, which is propagating southwestward along the Explorer/Pacific boundary to join the northern segment of the Juan de Fuca Ridge [*Bahr and Chase*, 1974; *Rohr and Furlong*, 1995]. No significant motion is accommodated along the former EX/NA boundary. This hypothesis is supported by seafloor morphology [*Rohr and Furlong*, 1995] and the current distribution of earthquakes in the eastern Explorer region [e.g., *Kreemer et al.*, 1998].

[82] In the first model, the interaction between the Explorer microplate and the North American plate should produce megathrust transient and/or permanent deformation signal in northern Vancouver Island. In the second model, all plate boundary deformation is accommodated offshore along the former Explorer spreading system, with very little to no elastic or permanent deformation expected in northern Vancouver Island.

4.2. Application to the Current GPS Velocities

[83] The distribution of continuous and campaign GPS sites in northern Vancouver Island is sparser than for the central and southern parts of the island. The measured displacement rates are also smaller, leading to higher uncertainties in the GPS data interpretation. Nevertheless, these data help discriminate between the two end-member models of EX/NA interaction.

[84] The NTKA and ELIZ permanent stations are located on the southern and northern sides of the Nootka Fault zone, respectively. Both stations are moving northeastward, similar to stations to the south, indicating that this motion is most likely related to strain accumulation along the locked subduction thrust (Figure 2). The velocity of NTKA can be accounted for by using the interseismic loading model 2 discussed in sections 3.1 and 3.2, with a JF/NA convergence velocity of 45 mm/yr toward N056° E (as predicted by the 0.4 Ma JF/NA rotation vector). The velocity of ELIZ roughly constrains the convergence rate between the Explorer and North America plates. Using an extension of model 2 north of the Nootka Fault (Figure 7), ELIZ velocity can be accounted for by an EX/NA convergence of about half the JF/NA rate in about the same direction. Because this conclusion relies on one GPS station with only 2 yrs of data, and because it is strongly dependent on the subduction model assumptions (e.g., type of transition zone decay), a more precise assessment of the EX/NA relative motion is not yet possible. However, the velocity pattern of the ELIZ and NTKA stations clearly indicates that the southern part of the Explorer plate is currently subducting underneath northern Vancouver Island (up to Brooks Peninsula), with strain accumulation along the subduction thrust. Assuming a fully locked subduction thrust on both sides of the Nootka Fault, the difference in subduction rate implies a left-lateral strike-slip rate along the Nootka Fault of ~20 mm/yr, similar to the rates estimated from plate motion models (25–35 mm/yr) [*Riddihough*, 1984; *Hyndman et al.*, 1979] and seismic moment release rate (10–30 mm/yr) [*Hyndman and Weichert*, 1983].

[85] Velocities of the campaign and continuous sites at the northern end of Vancouver Island and around the Queen Charlotte Strait are not significantly affected by the subduction-loading signal from the southern Explorer segment (Nootka Fault to Brooks Peninsula). Although the campaign velocities for the Queen Charlotte Strait network are not as spatially coherent as for the other networks, a systematic pattern of displacement can be observed (Figure 7). Most sites, including the three permanent stations, are moving roughly northward at ~2–4 mm/yr. This velocity field can be accounted for in two ways:

[86] 1. Assuming there is no current subduction underneath northernmost Vancouver Island, the GPS velocities would represent a nontransient signal indicating a small steady extension (northward motion) of northernmost Vancouver Island with respect to the southern part of the island. This extension is not supported by any earthquake or active fault data, but it could be connected to either the mid Neogene extension phase evidenced by volcanics (as late as Pliocene age [*Lewis et al.*, 1997]), or to the left-lateral

margin shear to the north in the Queen Charlotte Islands region [*Mazzotti et al.*, 2003].

[87] 2. Assuming active subduction underneath northernmost Vancouver Island, an ad hoc model of Winona/NA relative motion can be derived that would explain most of the GPS velocities as transient deformation due to the very oblique underthrusting of the Winona Block along a locked fault. Although this model does not account for the eastern GPS velocities (Queen Charlotte Strait-Inside Passage area), the residuals compared to the model predictions are very small (~2 mm/yr, Figure 7) and insignificant at the 95% level of confidence.

[88] Thus GPS data on northern Vancouver Island show that there is deformation, transient and/or permanent, along this part of the margin, consistent with the existence of an independent Explorer microplate and arguing against the hypothesis of the western Explorer region being attached to North America. This result is consistent with offshore earthquakes slip vectors that require a kinematically independent Explorer plate between Pacific and North America [*Ristau et al.*, 2002; *Braunmiller and Nábělek*, 2002]. However, GPS velocities are inconsistent with the EX/NA relative motion model proposed by *Braunmiller and Nábělek* [2002], which implies a southeastward subduction of the Explorer plate.

5. Conclusions

[89] On the basis of the analysis of 45 permanent GPS stations in the Cascadia Pacific Northwest and 67 campaign GPS measurements in the northern part of Cascadia, we have derived a consistent velocity field with respect to North America for NW Washington-SW British Columbia. There is good agreement between the continuous and campaign data. Horizontal GPS velocities range from 1–2 mm/yr for inland sites to over 10 mm/yr for coastal sites; the horizontal strain is well defined except at the most landward sites. In the vertical component, a pattern of general coastal uplift (~2 mm/yr) can be resolved. We estimate the velocity uncertainties using a model of time series noise spectrum [*Mao et al.*, 1999]. The modeled uncertainties for permanent stations are 0.5–1.0 mm/yr horizontal and 1.5–5 mm/yr vertical, depending mainly on the duration of the time series. For the campaign sites, the modeled uncertainties are ~1.5 mm/yr horizontal. Uncertainties for the vertical component are currently too large to be useful.

[90] The combined permanent campaign GPS velocities provide the basis for interpretation of the tectonics and kinematics of the northern Cascadia subduction system. The first order component of these velocities results from the interseismic loading of the Cascadia megathrust, and confirms that the upper part of the megathrust is fully, or nearly fully locked. An exponential transition zone downdip of the locked zone gives slightly better agreement with the data compared to the commonly used linear transition to free slip. However, the observed horizontal GPS velocities fall off landward more slowly than either model. This disagreement could be a consequence of a small (0–3 mm/yr) roughly northward long-term motion of the southern Vancouver Island forearc with respect to North America. Alternatively, it could be related to the existence of a weak crustal zone coincident with the volcanic belt, which may perturb the distribution of strain across the coastal margin.

[91] The goodness of fit of the tectonic models with the GPS velocities is estimated using a reduced χ^2 estimator. The best fit model (no forearc motion and exponential transition zone) shows a χ^2 improvement of about 25–50% compared to the alternative models. For the permanent station, the reduced χ^2 is relatively high (~4–13). This could indicate that the modeled uncertainties for the permanent station velocities are underestimated by a factor of 2–3. However, for all models the high χ^2 is due to large residuals at 2–4 stations, which vary from one model to another. Thus we suggest that the relatively large χ^2 mostly reflects the limitation of our simple elastic loading-rigid forearc models. The significant residuals at robust permanent station may indicate that the northern Cascadia forearc does not behave as a rigid elastic block and that local tectonic complications occur.

[92] In northern Vancouver Island, our GPS velocity field is consistent with the existence of an independent Explorer microplate currently underthrusting beneath North America, at least up to Brooks Peninsula. Further to the north, GPS velocities gradually rotate from nearly orthogonal to the margin toward the direction of the Pacific-North America relative motion. The vectors are consistent with an independent oblique underthrusting Winona Block, but also may be explained by permanent deformation within northern Vancouver Island, at the transition between the major subduction and transform systems.

[93] **Acknowledgments.** We gratefully acknowledge the Department of National Defense, the Canadian Coast Guard, and the National Research Council for their cooperation and assistance in the operation of continuous GPS stations at their various regional facilities in British Columbia. We are indebted to the Geodetic Survey Division of Geomatics Canada for their help in the development of WCDA infrastructure and their lead role in the execution of the GPS field campaigns. Continuous GPS data used in this study were also provided by Base Mapping and Geodetic Control, British Columbia, the PANGA GPS Network, and the BARD GPS Network. Reoccupation of two of the campaign networks was funded by NSF grant EAR-9814926 to RPI. Figures were prepared with GMT 3 software [*Wessel and Smith*, 1995]. This paper was greatly improved by reviews and discussions with R. King, J. Savage, T. Dixon, and I. Manighetti. Geological Survey of Canada contribution 2003113.

References

Altamimi, Z., P. Sillard, and C. Boucher, ITRF2000: A new release of the International Terrestrial Reference Frame for earth science applications, *J. Geophys. Res.*, *107*(B10), 2214, doi:10.1029/2001JB000561, 2002.

Atwater, B. F., and A. L. Moore, A tsunami about 100 years ago in Puget Sound, Washington, *Science*, *258*, 1614–1617, 1992.

Bahr, S. M., and R. L. Chase, Geology of the northern end of the Juan de Fuca Ridge and sea-floor spreading, *Can. J. Earth Sci.*, *11*, 1384–1406, 1974.

Braunmiller, J., and J. Nábělek, Seismotectonics of the Explorer region, *J. Geophys. Res.*, *107*(B10), 2208, doi:10.1029/2001JB000220, 2002.

Carbotte, S. M., J. M. Dixon, E. Farrar, E. E. Davis, and R. P. Riddihough, Geological and geophysical characteristics of the Tuzo Wilson seamounts: Implications for the plate geometry in the vicinity of the Pacific-North America-Explorer triple junction, *Can. J. Earth Sci.*, *26*, 2365–2384, 1989.

Cassidy, J. F., R. M. Ellis, C. Karavas, and G. C. Rogers, The northern limit of the subducted Juan de Fuca plate system, *J. Geophys. Res.*, *103*, 26,949–26,961, 1998.

Cattin, R., P. Briolle, H. Lyon-Caen, P. Bernard, and P. Pinettes, Effect of superficial layers on coseismic displacement for a dip-slip fault and geophysical implications, *Geophys. J. Int.*, *137*, 149–158, 1999.

Clague, J. J., and T. S. James, History and isostatic effects of the last ice sheet in southern British Columbia, *Quat. Sci. Rev.*, *21*, 71–87, 2002.

Currie, C. A., J. F. Cassidy, and R. D. Hyndman, A regional study of shear wave splitting above the Cascadia subduction zone: Margin-parallel crustal stress, *Geophys. Res. Lett.*, *28*, 659–662, 2001.

Davis, E. E., and R. P. Riddihough, The Winona Basin: Structure and tectonics, *Can. J. Earth Sci.*, *19*, 767–788, 1982.

DeMets, C., and T. H. Dixon, New kinematic models for the Pacific-North America motion from 3 Ma to present: I. Evidence for steady motion and biases in the NUVEL-1A model, *Geophys. Res. Lett.*, *26*, 1921–1924, 1999.

DeMets, C., R. G. Gordon, D. F. Argus, and S. Stein, Effects of recent revisions to the geomagnetic reversal time scale on estimates of current plate motions, *Geophys. Res. Lett.*, *21*, 2191–2194, 1994.

Dixon, T. H., M. M. Miller, F. Farina, H. Wang, and D. Johnson, Present-day motion of the Sierra Nevada block and some tectonic implications for the Basin and Range province: North American Cordillera, *Tectonics*, *19*, 1–24, 2000.

Dragert, H., and R. D. Hyndman, Continuous GPS monitoring of elastic strain in the northern Cascadia subduction zone, *Geophys. Res. Lett.*, *22*, 755–758, 1995.

Dragert, H., R. D. Hyndman, G. C. Rogers, and K. Wang, Current deformation and the width of the seismogenic zone of the northern Cascadia subduction thrust, *J. Geophys. Res.*, *99*, 653–668, 1994.

Dragert, H., X. Chen, and J. Kouba, GPS monitoring of crustal strain in southwest British Columbia with the Western Canada Deformation Array, *Geomatica*, *49*, 301–313, 1995.

Dragert, H., K. Wang, and T. S. James, A silent slip event on the deeper Cascadia subduction interface, *Science*, *292*, 1525–1528, 2001.

Dragert, H., S. Mazzotti, and K. Wang, Aseismic slip on the Northern Cascadia subduction zone: Impacts on seismic hazard estimates, *Eos Trans. AGU*, *83*(47), Fall Meet. Suppl., Abstract S21C-01, 2002.

Fletcher, H. J., J. Beavan, J. T. Freymueller, and L. Gilbert, High interseismic coupling of the Alaska subduction zone SW of the Kodiak Island inferred from GPS data, *Geophys. Res. Lett.*, *28*, 443–446, 2001.

Flück, P., R. D. Hyndman, and K. Wang, Three-dimensional dislocation model for great earthquakes of the Cascadia subduction zone, *J. Geophys. Res.*, *102*, 20,539–20,550, 1997.

Henton, J. A., GPS studies of crustal deformation in the northern Cascadia subduction zone, Ph.D. thesis, 169 pp., Univ. of Victoria, Victoria, B. C., Canada, 2000.

Henton, J. A., H. Dragert, R. D. Hyndman, and K. Wang, Geodetic monitoring of crustal deformation and strain on Vancouver Island, *Eos Trans. AGU*, *80*(46), Fall Meet. Suppl., Abstract G52A-09, 1999.

Henton, J. A., H. Dragert, R. McCaffrey, K. Wang, and R. D. Hyndman, North Cascadia margin deformation from GPS measurements, *Eos Trans. AGU*, *81*(48), Fall Meet. Suppl., Abstract G11A-14, 2000.

Hugentobler, U., S. Schaer, and P. Fridez (Eds.), Documentation of the Bernese GPS software version 4. 2, 511 pp., Astron. Inst., Univ. of Berne, Berne, 2001.

Hyndman, R. D., and K. Wang, The rupture zone of Cascadia great earthquakes from current deformation and thermal regime, *J. Geophys. Res.*, *100*, 22,133–22,154, 1995.

Hyndman, R. D., and D. H. Weichert, Seismicity and rates of relative motion on the plate boundaries of western North America, *Geophys. J. R. Astron. Soc.*, *72*, 59–82, 1983.

Hyndman, R. D., R. P. Riddihough, and R. Herzer, The Nootka Fault zone—A new plate boundary off western Canada, *Geophys. J. R. Astron. Soc.*, *58*, 667–683, 1979.

Hyndman, R. D., S. Mazzotti, D. Weichert, and G. C. Rogers, Large earthquake rate of occurrence in Puget Sound-S. Georgia Strait predicted from geodetic and geological deformation rates, *J. Geophys.*, 108, 2033, doi:10.1029/2001JB001710, 2003.

James, T. S., J. J. Clague, K. Wang, and I. Hutchinson, Postglacial rebound at the northern Cascadia subduction zone, *Quat. Sci. Rev.*, *19*, 1527–1541, 2000.

Johnson, S. Y., C. J. Potter, and J. M. Armentrout, Origin and evolution of the Seattle fault and Seattle basin, *Geology*, *22*, 71–74, 1994.

Khazaradze, G., A. Qamar, and H. Dragert, Tectonic deformation in western Washington from continuous GPS measurements, *Geophys. Res. Lett.*, *26*, 3153–3158, 1999.

Kleusberg, A., Y. Georgiadou, and H. Dragert, Establishment of crustal deformation networks using GPS: A case study, *CISM J. ACSGC*, *42*, 341–351, 1988.

Kreemer, C., R. Govers, K. P. Furlong, and W. E. Holt, Plate boundary deformation between the Pacific and North America in the Explorer region, *Tectonophysics*, *293*, 225–238, 1998.

Langbein, J., and H. Johnson, Correlated errors in geodetic time series: Implications for time-dependant deformation, *J. Geophys. Res.*, *102*, 591–604, 1997.

Le Provost, C., F. H. Lyard, J. M. Molines, M. L. Genco, and F. Rabilloud, A hydrodynamic ocean tide model improved by assimilating a satellite altimeter-derived data set, *J. Geophys. Res.*, *100*, 5513–5529, 1998.

Lewis, T. J., W. H. Bentowski, and R. D. Hyndman, Crustal temperature near the Lithoprobe southern Canadian Cordillera transect, *Can. J. Earth Sci.*, *29*, 1197–1214, 1992.

Lewis, T. J., C. Lowe, and T. S. Hamilton, Continental signature of a ridge-trench-triple junction: Northern Vancouver Island, *J. Geophys. Res.*, *102*, 7767–7781, 1997.

Mao, A., C. G. A. Harrison, and T. H. Dixon, Noise in GPS coordinate time series, *J. Geophys. Res.*, *104*, 2797–2816, 1999.

Mazzotti, S., X. Le Pichon, P. Henry, and S. Miyazaki, Full interseismic locking of the Nankai and Japan-west Kuril subduction zones: An analysis of uniform elastic strain accumulation in Japan constrained by permanent GPS, *J. Geophys. Res.*, *105*, 13,159–13,177, 2000.

Mazzotti, S., H. Dragert, R. D. Hyndman, M. M. Miller, and J. A. Henton, GPS deformation in a region of high crustal seismicity: N. Cascadia forearc, *Earth Planet. Sci. Lett.*, *198*, 41–48, 2002.

Mazzotti, S., R. D. Hyndman, P. Flück, A. J. Smith, and M. Schmidt, Distribution of the Pacific/North America motion in the Queen Charlotte Islands-S. Alaska plate boundary zone, *Geophys. Res. Lett.*, *30*(14), 1762, doi:10.1029/2003GL017586, 2003.

McCaffrey, R., Crustal block rotation and plate coupling, in *Plate Boundary Zone*, *Geodyn. Ser.*, vol. 30, edited by S. Stein and J. T. Freymueller, pp. 101–122, AGU, Washington, D. C., 2002.

McCaffrey, R., C. K. Johnson, P. C. Zwick, M. D. Long, C. Godfinger, J. L. Nabeleck, and C. Smith, Rotation and plate locking along the southern Cascadia subduction zone, *Geophys. Res. Lett.*, *27*, 3117–3120, 2000.

McCaffrey, R., A. Qamar, C. Williams, Z. Ning, P. Wallenberger, and R. W. King, Geodetic constraints on fault coupling on the Cascadia subduction zone, *Eos Trans. AGU*, *83*(47), Fall Meet. Suppl., Abstract S21C-06, 2002.

Miller, M. M., D. J. Johnson, C. M. Rubins, H. Dragert, K. Wang, A. Qamar, and C. Goldfinger, GPS-determination of along-strike variation in Cascadia margin kinematics: Implication for relative plate motion, subduction zone coupling, and permanent deformation, *Tectonics*, *20*, 161–176, 2001.

Miyazaki, S., and K. Heki, Crustal velocity field of southwest Japan: Subduction and arc-arc collision, *J. Geophys. Res.*, *106*, 4305–4326, 2001.

Mulder, T., Small earthquakes in southwestern British Columbia (1975–1991), M.Sc. thesis, 117 pp., Univ. of Victoria, Victoria, B. C., Canada, 1995.

Niell, A. E., Global mapping functions for the atmosphere delay at radio wavelengths, *J. Geophys. Res.*, *101*, 3227–3246, 1996.

Oleskevich, D. A., R. D. Hyndman, and K. Wang, The updip and downdip limits to great subduction earthquakes; thermal and structural models of Cascadia, south Alaska, SW Japan, and Chile, *J. Geophys. Res.*, *104*, 14,965–14,991, 1999.

Pagiatakis, S. D., Program LOADSDP for the calculation of ocean load effect, *Manusc. Geod.*, *17*, 315–320, 1992.

Reilinger, R., and J. Adams, Geodetic evidence for active landward tilting of the Oregon and Washington coastal ranges, *Geophys. Res. Lett.*, *9*, 401–403, 1982.

Riddihough, R. P., A model of recent plate interactions off Canada's west coast, *Can. J. Earth Sci.*, *14*, 384–396, 1977.

Riddihough, R. P., Recent movements of the Juan de Fuca plate system, *J. Geophys. Res.*, *89*, 6980–6994, 1984.

Riddihough, R. P., and R. D. Hyndman, Queen Charlotte Islands margin, in *The Geology of North America*, vol. N, *The Eastern Pacific Ocean and Hawaii*, edited by E. L. Winterer et al., pp. 403–411, Geol. Soc. of Am., Boulder, Colo., 1989.

Ristau, J., G. Rogers, and J. Cassidy, Slip direction and moment magnitude for earthquakes off Canada's west coast, *Eos Trans. AGU*, *83*(47), Fall Meet. Suppl., Abstract S71C-1113, 2002.

Rogers, G. C., and H. S. Hasegawa, A second look at the British Columbia earthquake of June 23, 1946, *Bull. Seismol. Soc. Am.*, *68*, 653–675, 1978.

Rohr, K. M. M., and K. P. Furlong, Ephemeral plate tectonics at the Queen Charlotte triple junction, *Geology*, *23*, 1035–1038, 1995.

Savage, J. C., and M. Lisowski, Strain measurements and potential for a great subduction earthquake off the coast of Washington, *Science*, *252*, 101–103, 1991.

Savage, J. C., M. Lisowski, and W. H. Prescott, Strain accumulation in western Washington, *J. Geophys. Res.*, *96*, 14,493–14,507, 1991.

Sella, G. F., T. H. Dixon, and A. Mao, REVEL: A model for Recent plate velocities from space geodesy, *J. Geophys. Res.*, *107*(B4), 2081, doi:10.1029/2000JB000033, 2002.

Svarc, J. L., J. C. Savage, W. H. Prescott, and M. H. Murray, Strain accumulation and rotation in western Oregon and southwestern Washington, *J. Geophys. Res.*, *107*(B5), 2087, doi:10.1029/2001JB000625, 2002.

Wahlström, R., and G. C. Rogers, Relocation of earthquakes west of Vancouver Island, British Columbia, 1965–1983, *Can. J. Earth Sci.*, *29*, 953–961, 1992.

Walcott, D., Neogene tectonics and kinematics of western North America, *Tectonics*, *12*, 326–333, 1993.

Wang, K., R. Wells, S. Mazzotti, R. D. Hyndman, and T. Sagiya, A revised dislocation model of interseismic deformation of the Cascadia subduction zone, *J. Geophys. Res.*, *108*(B1), 2026, doi:10.1029/2001JB001227, 2003.

Wells, R. E., C. S. Weaver, and R. J. Blakely, Forearc migration in Cascadia and its neotectonic significance, *Geology*, *26*, 759–762, 1998.

Wessel, P., and W. H. F. Smith, New version of the Generic Mapping Tools released, *Eos Trans. AGU*, *76*, 329, 1995.

Wilson, D. S., Confidence intervals for motion and deformation of the Juan de Fuca plate, *J. Geophys. Res.*, *98*, 16,053–16,071, 1993.

Wolynec, L., H. Dragert, A. Lambert, M. Schmidt, and A. Mainville, Improving model constraints for vertical deformation across the northern Cascadia margin, paper presented at Annual CGU Meeting, Can. Geophys. Union, Banff, Alberta, 2003.

Yoshioka, S., K. Wang, and S. Mazzotti, Locking state of the northern Cascadia megathrust fault inferred from inversion of GPS velocities, *Eos Trans. AGU*, *82*(47), Fall Meet. Suppl., Abstract G41A-0189, 2001.

Zhang, J., Y. Bock, H. Johnson, P. Fang, S. Williams, J. Genrich, S. Wdowinski, and J. Behr, southern California permanent GPS geodetic array: Error analysis of daily position estimates and site velocities, *J. Geophys. Res.*, *102*, 18,035–18,055, 1997.

M. Craymer and J. Henton, Gravity and Geodetic Networks Section, Geodetic Survey Division, 615 Booth Street, Ottawa, Ontario, Canada K1A 0E9. (mcraymer@nrcan.gc.ca; jhenton@nrcan.gc.ca)

H. Dragert, R. Hyndman, T. James, Y. Lu, S. Mazzotti, and M. Schmidt, Pacific Geoscience Centre, Geological Survey of Canada, 9860 West Saanich Road, Sidney, British Columbia, Canada V8L 4B2. (dragert@pgc.nrcan.gc.ca; rhyndman@nrcan.gc.ca; james@pgc.nrcan.gc.ca; lu@pgc.nrcan.gc.ca; smazzotti@nrcan.gc.ca; mschmidt@nrcan.gc.ca)